

## Article

# TGF $\beta$ Inhibitor A83-01 Enhances Murine HSPC Expansion for Gene Therapy

Jenni Fleischauer<sup>1,2</sup>, Antonella Lucia Bastone<sup>1,2</sup>, Anton Selich<sup>1,2</sup>, Philipp John-Neek<sup>1,2</sup>, Luisa Weisskoeppel<sup>1,2</sup>, Dirk Schaudien<sup>3</sup>, Axel Schambach<sup>1,2,4</sup> and Michael Rothe<sup>1,2,\*</sup>

<sup>1</sup> Institute of Experimental Hematology, Hannover Medical School, 30625 Hannover, Germany; fleischauer.jenni@mh-hannover.de (J.F.); bastone.antonella@mh-hannover.de (A.L.B.); selich.anton@mh-hannover.de (A.S.); john-neek.philipp@mh-hannover.de (P.J.-N.); weisskoeppel.luisa@mh-hannover.de (L.W.); schambach.axel@mh-hannover.de (A.S.)

<sup>2</sup> REBIRTH—Research Center for Translational Regenerative Medicine, Hannover Medical School, 30625 Hannover, Germany

<sup>3</sup> Department of Inhalation Toxicology, Fraunhofer Institute for Toxicology and Experimental Medicine ITEM, Nikolai Fuchs Strasse 1, 30625 Hannover, Germany; dirk.schaudien@item.fraunhofer.de

<sup>4</sup> Division of Hematology/Oncology, Boston Children's Hospital, Harvard Medical School, 30625 Hannover, Germany

\* Correspondence: rothe.michael@mh-hannover.de; Tel.: +49-511-532-5137

**Abstract:** Murine hematopoietic stem and progenitor cells (HSPCs) are commonly used as model systems during gene therapeutic retroviral vector development and preclinical biosafety assessment. Here, we developed cell culture conditions to maintain stemness and prevent differentiation during HSPC culture. We used the small compounds A83-01, pomalidomide, and UM171 (APU). Highly purified LSK SLAM cells expanded in medium containing SCF, IL-3, FLT3-L, and IL-11 but rapidly differentiated to myeloid progenitors and mast cells. The supplementation of APU attenuated the differentiation and preserved the stemness of HSPCs. The TGF $\beta$  inhibitor A83-01 was identified as the major effector. It significantly inhibited the mast-cell-associated expression of Fc $\epsilon$ R1 $\alpha$  and the transcription of genes regulating the formation of granules and promoted a 3800-fold expansion of LSK cells. As a functional readout, we used expanded HSPCs in state-of-the-art genotoxicity assays. Like fresh cells, APU-expanded HSPCs transduced with a mutagenic retroviral vector developed a myeloid differentiation block with clonal restriction and dysregulated oncogenic transcriptomic signatures due to vector integration near the high-risk locus *Mecom*. Thus, expanded HSPCs might serve as a novel cell source for retroviral vector testing and genotoxicity studies.

**Keywords:** hematopoietic stem and progenitor cells; stem cell expansion; A83-01; TGFbeta signaling; mast cells; gene therapy; genotoxicity; IVIM; SAGA



**Citation:** Fleischauer, J.; Bastone, A.L.; Selich, A.; John-Neek, P.; Weisskoeppel, L.; Schaudien, D.; Schambach, A.; Rothe, M. TGF $\beta$  Inhibitor A83-01 Enhances Murine HSPC Expansion for Gene Therapy. *Cells* **2023**, *12*, 1978. <https://doi.org/10.3390/cells12151978>

Academic Editors: Albert Rizvanov and Ayşegül Doğan

Received: 7 July 2023

Revised: 28 July 2023

Accepted: 28 July 2023

Published: 31 July 2023



**Copyright:** © 2023 by the authors. Licensee MDPI, Basel, Switzerland. This article is an open access article distributed under the terms and conditions of the Creative Commons Attribution (CC BY) license (<https://creativecommons.org/licenses/by/4.0/>).

## 1. Introduction

Monogenic disorders, such as primary immune deficiencies [1,2], hemoglobinopathies [3–5], bone marrow failure syndromes [6–8], and lysosomal storage diseases [9,10], cause life-threatening symptoms. Ex vivo gene correction with retroviral vectors and transplantation of genetically modified cells were effective in clinical trials for such disorders and could reduce disease symptoms. To develop new gene therapy vectors, mouse hematopoietic stem and progenitor cells (HSPCs) serve as crucial model systems for gene modification. Finding expansion protocols for HSPCs would be desirable to reduce the need for animal donors. Ex vivo cultivation outside the bone marrow (BM) niche can lead to rapid differentiation and the loss of long-term engraftable hematopoietic stem cells (HSCs). Thus, improvements in HSC cultivation for gene modification and reliable safety assays of retroviral vectors are essential for the clinical translation of new gene therapy strategies according to 3R principles.

To maintain the stemness of HSPCs after ex vivo gene correction, media with cytokines mimicking the microenvironment of the stem cell niche are the basis of expansion protocols. Specific combinations of key cytokines, such as stem cell factor (SCF), interleukin 3 (IL-3), IL-11, IL-6, and FMS-like tyrosine kinase 3 ligand (FLT3-L), can highly influence the phenotype of the expanded HSPCs [11,12], their proliferation capacity, and their long-term engraftment. Lui and colleagues showed how media supplemented with SCF, IL-3, and IL-6 promoted high numbers of phenotypically short-term HSCs (lineage-negative [lin<sup>-</sup>] Sca1+cKit<sup>+</sup>, LSK), with the majority of these cells expressing the Fc epsilon receptor 1 alpha (FcεR1α<sup>+</sup>), typical for mast cells. By exchanging IL-3 and IL-6 for FLT3-L and IL-11, they significantly reduced the percentage of mast cells in culture. However, this came along with a reduction in LSK cell expansion.

In this study, we initially evaluated four different media and their ability to expand murine BM-derived LSK SLAM (LSK CD48<sup>-</sup> CD150<sup>+</sup>) cells. The best candidate contained the cytokines SCF, IL-3, FLT3-L, and IL-11 (S3F11), but expectedly led to the differentiation of myeloid progenitors and mast cells. Thus, we supplemented S3F11 with the small molecules A83-01, pomalidomide, and UM171 (S3F11+APU) to target signaling pathways that induce HSC propagation and counteract quiescence [13]. A83-01 inhibits TGFβ signaling by targeting activin receptor-like kinase 5 (ALK5, TGFβ type I receptor), ALK4 (type I activin/nodal receptor), and ALK7 (type I nodal receptor), which consequently blocks the phosphorylation of Smad2 [14,15]. Since high concentrations of TGFβ promote quiescence in HSCs, we hypothesized that inhibition with A83-01 would lower the levels of TGFβ and allow the cycling of HSCs [16,17]. Additionally, we used pomalidomide to influence Notch signaling, which stimulates HSC self-renewal [18,19]. Notch is negatively regulated by the transcription factor Ikaros [20–22]. In the context of multiple myeloma, thalidomide and its derivate pomalidomide could promote the degradation of Ikaros by altering the substrate specificity of cereblon (CRBN), the target of the CUL4-RBX1-DDB1-CRBN (also known as CRL4<sup>CRBN</sup> E3 ubiquitin ligase. Upon pomalidomide treatment, CRL4<sup>CRBN</sup> degrades neosubstrates, such as Ikaros, instead of its endogenous targets, such as MEIS2 [23,24]. Furthermore, we used the small molecule UM171, which has proven to maintain stemness and proliferation in human and murine HSPC expansion protocols [25–27]. Our data suggest that the TGFβ inhibitor A83-01 primarily maintained murine HSPC attributes and an arrest of differentiation. A83-01 significantly attenuated mast cell differentiation while promoting LSK cell expansion. Thus, we underline the importance of TGFβ in hematopoiesis, especially the effect on the cycling state of HSCs [28].

We tested the functionality of expanded HSPC in two in vitro genotoxicity tests. The in vitro immortalization (IVIM) assay [29] and the surrogate assay for genotoxicity (SAGA) [30] assess the mutagenic potential of retroviral vectors on murine BM-derived lin<sup>-</sup> cells (Scheme I). The IVIM assay quantifies the outgrowth of insertion mutants after a low cell density replating step. SAGA determines the dysregulation of genes associated with the in vitro transformation of murine HSPCs. Both assay systems rely on primary mouse cells. We were determined to use expanded cell material as input in the assays to reduce the number of animals needed as donors. Despite a reduced frequency of clonal outgrowth, APU-expanded (-Exp) cells harbored characteristic high-risk insertions near the *MDS1* and *EV11 complex locus (Mecom)* when transduced with a mutagenic vector, reflecting the main findings of previous IVIMs with nonexpanded cells. It is noteworthy that the immune phenotyping of expanded cells transduced with oncogenic vectors showed a differentiation block of early myeloid progenitors. Safer vector designs did not lead to the immortalization of fresh or expanded cells in IVIM. SAGA revealed a similar enrichment of stemness- and transformation-associated genes after oncogenic vector transduction in APU-Exp and fresh lin<sup>-</sup> cells.

In summary, our work shows how cells cultivated in A83-01 retain a stem-cell-like phenotype after expansion, making them suitable for testing retroviral vector transduction efficiency, control of the long-term transgene expression, and genotoxicity studies.

## 2. Materials and Methods

### 2.1. LSK SLAM Sorting and Expansion

BM cells were harvested by flushing tibiae, femora, and iliac crests of 8- to 12-week old female C57BL/6J mice (Janvier, Pays de la Loire, France). Erythrocytes were lysed by incubating the BM cell suspension in red blood cell lysis buffer (1.5 M ammonium chloride, 100 mM potassium hydrogen carbonate, and 10 mM disodium EDTA in distilled water with pH = 7.2) for 10 min (1.5 mL/mouse). The reaction was stopped by washing with magnetic-activated cell sorting (MACS) buffer (0.5% FCS (PAN Biotech, Aidenbach, Germany)) and 2 mM EDTA (PAN Biotech) in DPBS (PAN Biotech). Purified cells were depleted for hematopoietic lin markers (CD5, CD45R, CD11b, Anti-Gr-1 (also known as Ly6G), 7-4, and Ter-119) by MACS according to the manufacturer's protocol (Miltenyi Biotec, Bergisch Gladbach, Germany, Catalogue No. 130-090-858). Before FACS staining, lin-depleted cells were incubated for 15 min with 0.5 µg CD16/CD32 antibody (eBioscience, San Diego, CA, USA, Catalogue No. 14-0161-82) in FACS buffer consisting of PBS (PAN Biotech) supplemented with 2% FCS (PAN Biotech) and 2 mM EDTA (PAN Biotech) to prevent unspecific antibody binding. To obtain lin- cells, lin-depleted BM cells were stained with the "Biotin anti-mouse Lineage Panel" (Anti-CD11b, -GR1 (also known as Ly6g), -Ter119, -CD3e, and -CD45R) provided by BioLegend (Catalogue No. 133307) and coupled to streptavidin BV785 (BioLegend, San Diego, CA, USA, Catalogue No. 405249). LSK SLAM cells were identified by staining with anti-cKit/APC-Cy7 (BioLegend, Catalogue No. 105826), anti-Sca-1/PerCP-Cy5.5 (eBioscience, Catalogue no.45-5981-82), anti-CD48/FITC (BioLegend, Catalogue No. 103404), and anti-CD150/PE-Cy7 (BioLegend, Catalogue No. 115914). Finally, samples were resuspended in 0.2 µg/mL DAPI (Sigma-Aldrich, Saint Louis, MO, USA, Catalogue No. D9542) for dead cell exclusion. FACS was performed with the FACS Aria Fusion cell sorter (Becton Dickinson, Franklin Lakes, NJ, USA), and analyses were performed with FACSDiva, Version 8.0.1 software (Becton Dickinson). Sorted LSK SLAM cells or lin-depleted cells were seeded in a 96-well flat-bottom plate for suspension cells (Sarstedt, Nümbrecht, Germany) with a cell density of 50 cells/well in different expansion media: STIF, SFT, S3F11, S3F11T, and S3F11+APU (media and concentrations in Supplementary Table S1). Half-medium changes were performed twice weekly, and wells were expanded if confluence reached 70%.

### 2.2. MTT Assay

MTT assay was used to determine the number of expanded cells by correlating the metabolic activity to a standard curve of lin- cells. For the IVIM assay, the absorbance was compared with the microscopical scoring. Thus, cells were stained with 0.25% thiazolyl blue tetrazolium bromide (MTT, Sigma) in DPBS (Pan Biotech) for 2–3 h at 37 °C before lysing the cells in 10% SDS (Sigma). Plates were incubated while shaking overnight at RT. Absorption was measured at 540 nm with the plate reader SpectraMax 340PC (Molecular Devices, San Jose, CA, USA).

### 2.3. Flow Cytometry

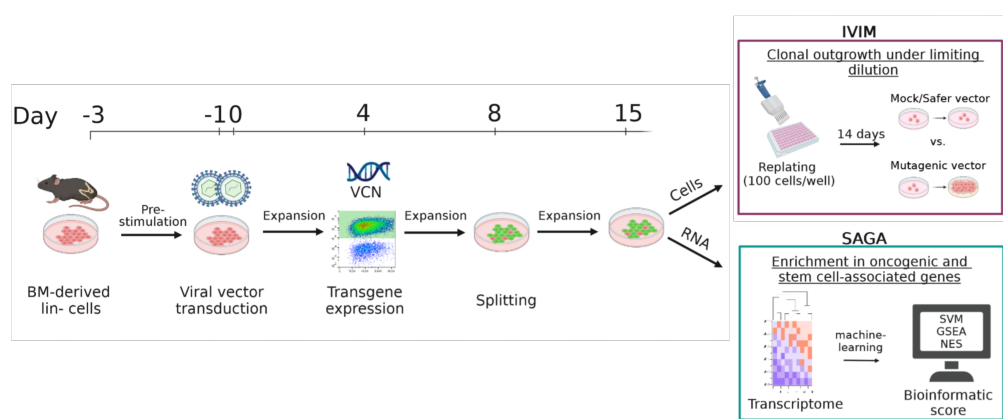
The immune surface phenotype was assessed for myeloid, lymphoid, mast cell, and multipotent HSPC marker: Anti-CD3ε/APC-Cy7 (BioLegend Catalogue no.100330), anti-B220-APC/Cy7 (BioLegend Catalogue No. 103224), anti-Ter119/APC-Cy7 (BioLegend Catalogue No. 103224), anti-CD11b/AF700 (BioLegend Catalogue No. 103224), anti-Gr1 (BioLegend Catalogue No. 108422), anti-FcεR1α/FITC (eBioscience Catalogue No. 11-5898-85) or anti-FcεR1α/PE (eBioscience, Catalogue No. 12-5898-83), anti-cKit/APC-Cy7 (BioLegend, Catalogue No. 105826), and anti-Sca-1/PerCP-Cy5.5 (eBioscience, Catalogue No. 45-5981-82). Samples were finally stained within 0.2 µg/mL DAPI (Sigma-Aldrich, Catalogue No. D9542) for dead cell exclusion. Flow cytometry was performed with the Cytotoflex S (Beckman Coulter, Brea, CA, USA) cytometer, and data were analyzed with the CytExpert (Beckman Coulter) and FlowJo, Version 10.2 (Tree Star, Ashland, OR, USA) software.

## 2.4. Cytospin Analysis

For microscopic analysis of cytopins,  $5 \times 10^4$  cells were centrifuged for 10 min at 800 rpm on microscopic slides using the Thermo Shandon Cytospin 4 centrifuge (Thermo Fisher Scientific, Waltham, MA, USA). For the Pappenheim staining, cells were stained 5 min in May-Grünwald dye, washed, and then stained for 20 min in Giemsa dye (Sigma-Aldrich). Cytopins were visualized with a NanoZoomer S210 digital slide scanner (Hamamatsu, Hamamatsu City, Japan) using  $40\times$  magnification. Cell morphology was assessed with the NDP.view2 2.8.24 viewing software U12388-01 (Hamamatsu).

## 2.5. In Vitro Immortalization Assay

Cell-culture-based assay was used to determine the genotoxic risk of retroviral vectors as previously described [29,30]. In brief, BM-derived lin- cells were thawed and prestimulated for 2 days in serum-free StemSpan™ SFEM (STEMCELL Technologies, Vancouver, BC, Canada) supplemented with S3F11 cytokines before transduction (Scheme 1).



**Scheme 1.** The In Vitro Immortalization (IVIM) and Surrogate Assay for Genotoxicity Assessment (SAGA). Graphical illustration of the standard operating protocol for the IVIM assay and SAGA. Murine BM-derived lin-depleted cells were thawed, prestimulated, and transduced in two rounds with retroviral vectors. Transgene expression and vector copy number (VCN) were determined for transduction efficiency on day 4 post-transduction. After several days of expansion and one splitting step, cells were replated on day 15 in low cell density (100 cells/well) to detect immortalization events in vitro by determining clonal outgrowth after 14 days. RNA was harvested for transcriptome analysis via microarray. Machine learning predicted a classification of vector mutagenicity by a support vector machine (SVM), gene set enrichment analysis (GSEA), and a normalized enrichment score (NES).

For this study, cells were modified either with an LTR-driven gammaretroviral vector encoding a fluorophore as a positive control named RSF91 (previously described here [31–33]), a SIN lentiviral vector with an EFS promoter (abbreviated as EFS and described here [34,35]), or remained untransduced (mock). On day 15 post-transduction, 100 cells/96-well (flat-bottom suspension plate) were replated for another 2-week culture period. Afterward, plates were screened for wells showing clonal transformation. In addition, the metabolic activity was measured by MTT to determine the number of positive wells showing transformation and the replating frequency.

## 2.6. VCN Determination by qPCR

Vector copy number (VCN) per diploid cell was determined by quantifying the amount of vector-derived woodchuck hepatitis virus post-transcriptional regulatory element (WPRE) compared with genomic polypyrimidine tract binding protein 2 (PTBP2) by Taqman qPCR on an Applied Biosystems StepOnePlus System (Foster City, CA, USA). Thus, 100 ng of genomic DNA from transduced (RSF91, EFS) and mock samples were used per PCR reaction. The ABI Taqman Fast Advanced Master Mix (Thermo Fisher Scientific)

was used with 660 nM WPRE and PTBP2 primer and 150 nM of the respective probes. The PCR was run in 40 cycles.

### 2.7. Surrogate Assay for Genotoxicity Assessment

We previously developed the machine learning algorithm “surrogate assay for genotoxicity assessment” (SAGA) to predict the mutagenic risk of viral vectors for clinical studies [30,36]. Cells were harvested for RNA isolation on day 15 of the IVIM assay (Scheme 1). Thus, a cell pellet of half of the bulk was frozen in 350 µL RLT lysis buffer (Qiagen). RNA was isolated with the RNeasy kit (Qiagen) according to the manufacturer’s protocol. RNA was transferred to the research core unit genomics (RCUG) of the Hannover Medical School for quality control using the 2100 Bioanalyzer (Agilent) and microarray analysis with the microarray scanner G2565CA (Agilent). Probes were annotated to the Whole Mouse Genome Oligo Microarray 4 × 44 K v2 and mapped to 60mer sequences to a recent release of the murine transcriptome (Gencode version M181, GRCm38.p6, release 07/2018). SAGA analysis was performed with R 4.2.0, Bioconductor 3.15, and the R package “saga” described here: [https://talbotsr.com/saga\\_package/index.html](https://talbotsr.com/saga_package/index.html) (accessed on 5 July 2023). The whole code can be downloaded from Github ([https://github.com/mytalbot/saga\\_package/](https://github.com/mytalbot/saga_package/), accessed on 5 July 2023). In brief, sample information was given in the “SampleInformation” .txt file before importing microarray .txt files to the SAGA pipeline. Raw data were preprocessed by quantile normalization and batch correction. Transforming and untransforming vectors were discriminated by principal component analysis (PCA) using the support vector machine (SVM), which is based on 20 predictors for genotoxicity. Gene set enrichment analysis (GSEA) revealed a normalized enrichment score (NES), which classifies the enrichment of 11 predictors within transduced samples compared with mock. Safer vectors usually score an NES < 1, whereas mutagenic vectors have a high NES > 1.

### 2.8. Insertion Site Analysis with INSPIRED

INSPIRED (integration site pipeline for paired-end reads) is a pipeline developed by Berry and colleagues to determine vector integration sites [37]. Genomic DNA was isolated from IVIM bulk (day 15 or day 21) or clones using the DNeasy Blood and Tissue Kit (Qiagen). DNA was sheared by sonification using the S220 Focused-ultrasonicator (Covaris, Woburn, MA, USA). Purification was performed with AMPure Beads (Beckman and Coulter) in a 0.7-fold ratio. Fragmented DNA was end-repaired with the NEBNext Ultra II End Repair/dA-Tailing Module (New England Biolabs (NEB), Frankfurt, Germany) and ligated with specific linkers using the NEBNext Ultra II Ligation Module (NEB). After following the same purification procedure with the AMPure Beads, nested PCRs were run to amplify the vector-genome junctions by adding Illumina adapter sequences, using specific index primers and sample-specific linker primers. The PCR products were visualized on 2% agarose gels, measured by Qubit, and pooled into DNA libraries that were transferred to the RCUG of the Hannover Medical School for quality control with a Bioanalyzer device and analysis by Illumina sequencing on flow cells with 1 million clusters. Linker and primer sequences used for PCR reactions are available upon request. Downstream bioinformatic processing was generally performed as described by Berry and colleagues [37]. The analysis files necessary to run the INSPIRED pipeline were downloaded from GitHub (<https://github.com/BushmanLab/INSPIRED>, accessed on 5 July 2023). Demultiplexed sequences in FASTQ format were generated according to the individual index primers used, quality checked, aligned, and annotated to the mouse genome (mm9). The plasmid vector sequences served as a reference for LTR regions and vector trimming. The processing and alignment statistics were exported before uploading the results to a local database. After creating a sample management database, reports with all integration site data were generated and used for customized postprocessing in Excel, Version 2016 and GraphPad Prism, Version 9 (GraphPad Prism Incorporation, San Diego, CA, USA).

### 2.9. Transcriptome Analysis

RNA was isolated from 2-week expanded material and used for microarray analysis, likewise described above. S3F11-Exp cells were compared with S3F11+A83-01-Exp cells for significantly differentiated cells ( $p < 0.05$ ). The R packages “limma”, “fgsea”, “RColorBrewer”, “gplots”, and “ggplot2” were used to generate heat maps and volcano plots. Gene set enrichment analysis was performed using the ontology M5 gene sets from the Mouse Molecular Signatures Database (MSigDB) and filtered for expected hematopoietic cell types (“hematopoietic”, “mast\_cell”, “myelo”, “monocyte”, “lymphoid”, “erythro”, “macrophage”, “leuko”, “platelet”, “neutrophil”, “granulocyte”) and key words of the TGF $\beta$  signaling pathway (“transforming\_growth\_factor”, “activin\_receptor”, “smad”, “epithelial\_to\_mesenchymal\_transition”, “MAPK”).

### 2.10. Protein Extraction and Western Blot Analysis

Inhibition of TGF $\beta$  signaling was analyzed based on the protein level of phospho-Smad2/3. Cells expanded for 2 weeks in S3F11 or S3F11+A/APU were lysed in RIPA buffer (150 mM NaCl, 50 mM Tris-HCl, 1% Nonidet P-40, 0.5% sodium deoxycholate, 0.1% SDS in ddH<sub>2</sub>O) supplemented with a protease inhibitor (cComplete<sup>TM</sup>, Mini Protease Inhibitor Cocktail, Roche). Based on the Bradford method, the protein concentration was determined with the Bio-Rad Protein Assay Dye Reagent Concentrate (Catalogue No. 500000630). An amount of 30  $\mu$ g protein was loaded on a 12.5% SDS polyacrylamide gel and blotted on a nitrocellulose membrane. Phospho-Smad2 was detected by the respective primary antibody (anti-phospho-Smad2, Ser465/467, rabbit polyclonal, 1:500, Sigma-Aldrich, Catalogue No. AB3849-I) and HRP-conjugated anti-rabbit IgG secondary antibody (1:4000, Cayman Chemical Company, Ann Arbor, MI, USA, Catalogue No. 10004301) for detection. Normalization was performed based on the housekeeping protein vinculin (anti-vinculin, mouse monoclonal, 1:20,000, Sigma, V9131) visualized by HRP-conjugated anti-mouse IgG secondary antibody (1:4000, Cayman Chemical Company, Catalogue No. 10004302). The SuperSignal<sup>TM</sup> West Pico PLUS Chemiluminescent Substrate (Thermo Scientific, Catalogue No. 34580) was added to the membranes for chemiluminescent detection. The Fusion FX7 (Vilber Lourmat) device acquired imaging, and protein bands were quantified based on their densitometry with the FusionCapt Advance Solo 4 16.07 software (Vilber Lourmat, Marne La Vallée, France).

## 3. Results

### 3.1. Massive Ex Vivo Expansion in S3F11+APU Medium after LSK SLAM Purification

We aimed to expand primary murine HSPCs to use them in preclinical gene therapy safety assays. However, increased in vitro proliferation of HSPCs often leads to their differentiation. Hence, we sought to find culture conditions that preserve the HSPC phenotype characterized by the absence of a lineage marker (CD5, CD45R, CD11b, Anti-Gr-1 (also known as Ly6G), 7-4, and Ter-119) and the expression of cKit and Sca-1 (LSK), while increasing the overall cell pool. In our initial screen, we explored four different cytokine combinations (STIF, SFT, S3F11, and S3F11T described in Supplementary Table S1) for the ex vivo expansion of BM-derived HSPCs. We compared the expansion potential of seeding either highly purified LSK SLAM cells, likewise described by Wilkinson and colleagues [38], or lin- cells from murine bone marrow in low cell density (50 cells/96-well) (Figure 1A).

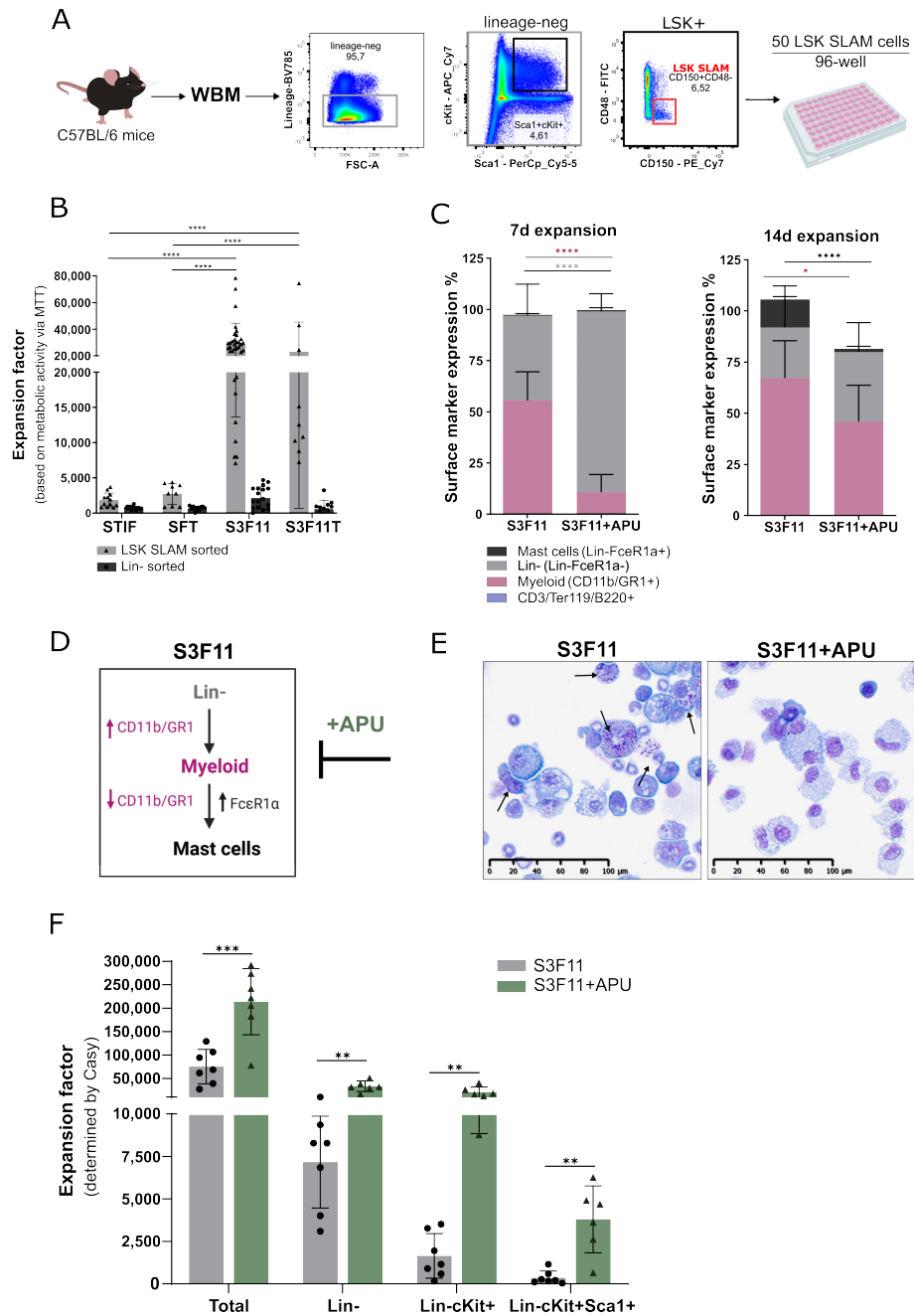


**Figure 1.** Massive ex vivo expansion after seeding LSK SLAM cells for 14 days in S3F11+APU medium. (A) Murine whole bone marrow (WBM) was depleted for cells expressing hematological lin markers (CD5, CD45R, CD11b, Anti-Gr-1, 7-4, and Ter-119) and enriched for LSK (lin-Sca+cKit+) and SLAM (CD48- CD150+) markers. LSK SLAM cells were cultured in a low cell density setting (50 cells/96 well). (B) Expansion factor of HSPCs after cultivating 50 LSK SLAM or 50 lin- cells in different cytokine conditions. Cell number was estimated based on metabolic activity measured with MTT dye. A standard curve with a set number of cells was performed for extrapolation. After 2 weeks of expansion in STIF, SFT, S3F11, or S3F11T medium, only medium containing S3F11(T) cytokines led to significantly higher expansion (over 20,000-fold, n = 3) if HSPCs were purified for an LSK SLAM marker. Statistical analysis performed with two-way ANOVA and Bonferroni multiple comparisons comparing media within sorted population. STIF: SCF, TPO, IGF2, FGF2 in StemSpan SFEMI; SFT: SCF, FLT3-L, TPO in StemSpan SFEMI; S3F11: SCF, IL-3, FLT3-L, IL-11 in IMDM+10%

FCS; S3F11T: SCF, IL-3, FLT3-L, IL-11, TPO in IMDM+10% FCS. (C) Mean ( $n = 3$ ) of surface marker contribution after 7 and 14 days in the respective medium. Adding APU (A83-01, pomalidomide, UM171) to the S3F11 medium maintained the presence of lin<sup>-</sup> cells, restrained myeloid (CD11b/GR1<sup>+</sup>) cells on day 7, and attenuated FcεR1α expression until day 14. Statistical analysis performed with Mann–Whitney test. (D) Graphical illustration of the dynamic marker expression during mast cell development in S3F11 medium and the inhibitory influence of A83-01. (E) May–Grünwald Giemsa staining of expanded cells on day 14. The arrows indicate representative cells with dark cytosolic granules typical for mast cells. 20× magnification, 100 μm scale bar. (F) Expansion factor (number of expanded cells divided by seeded number of 50 LSK SLAM cells) of total, lin<sup>-</sup>, lin-cKit<sup>+</sup>, and lin-cKit<sup>+</sup>Sca1<sup>+</sup> cells after 2 weeks in S3F11 or S3F11+APU medium ( $n = 3$ ). Cell numbers were assessed by Casy. Significantly more total, lin<sup>-</sup>, lin-cKit<sup>+</sup>, and LSK<sup>+</sup> cells were expanded in S3F11+APU. Two-way ANOVA with Tukey's correction for multiple testing. "n" is the number of biological replicates; error bars correspond to SD;  $p < 0.05 = *$ ,  $p < 0.01 = **$ ,  $p < 0.01 = ***$ ,  $p < 0.0001 = ****$ , and without label if  $p > 0.05 =$  not significant.

HSPC expansion was estimated with a fold change of over 20,000 in S3F11(T)medium based on their metabolic activity in the MTT assay, but only if they were sorted for LSK SLAM (Figure 1B). Sorting only for lin<sup>-</sup> cells was not sufficient for notable expansion in low cell density. Therefore, HSPCs were always purified for LSK SLAM markers before ex vivo expansion. Since the addition of thrombopoietin (T) resulted in the same expansion as seen in S3F11, it was neglected in the following experiments. Despite the massive expansion, S3F11 medium induced rapid differentiation of LSK SLAM cells towards the myeloid lineage (55.5% CD11b/GR1<sup>+</sup> until day 7), followed by downregulation of myeloid markers and accompanied FcεR1α expression (13.8%) until day 14 (Figure 1C). The small compounds APU have been shown to expand human CD34<sup>+</sup> cells while maintaining their stemness successfully [13]. We hypothesized that adding APU to the S3F11 medium (S3F11+APU) might decrease the differentiation of murine HSPCs while they continue to proliferate. Indeed, on day 7 of expansion in S3F11+APU, still 88.3% of the population remained lin<sup>-</sup> in contrast to the significantly reduced lin<sup>-</sup> population in S3F11 medium (41.5%,  $p < 0.0001$ , Figure 1C). Even on day 14 of expansion, S3F11+APU-Exp cells still contained 10% more lin<sup>-</sup> cells than S3F11-Exp cells. Additionally, the presence of myeloid progenitors was significantly reduced by 21.1% in the S3F11+APU medium until day 14 ( $p > 0.01$ ). After 14 days of expansion, 13.8% of S3F11-Exp cells expressed the mast cell marker FcεR1α, which was also significantly attenuated by the addition of APU (<2% FcεR1α<sup>+</sup> in S3F11+APU,  $p < 0.0001$ ). The dynamic marker expression is summarized in Figure 1D. Histopathology confirmed the presence of characteristic cytosolic mast cell granules in S3F11-Exp cultures (Figure 1E, black arrows) and the absence in the S3F11+APU medium. The expansion factor was assessed quantitatively using the Casy counting device and showed in addition to the mast cell attenuation an over 200,000-fold expansion of the total cell population, 30,000-fold expansion of lin<sup>-</sup> cells, around 20,000-fold expansion of lin-cKit<sup>+</sup> cells, and 3800-fold expansion of LSK cells in S3F11+APU, significantly higher than in S3F11 only (Figure 1F,  $p < 0.001$  for total and  $p < 0.01$  for lin<sup>-</sup>, lin-cKit<sup>+</sup>, and LSK cells).

### 3.2. A83-01 Is the Key Compound to Attenuate Mast Cell Differentiation

To resolve which compound in the APU cocktail inhibits mast cell differentiation (Figure 1B), we expanded LSK SLAM cells in single and minus-one compound combinations for 2 weeks and monitored the distribution of mast cells, myeloid cells, and lin<sup>-</sup> cells (Figure 2A–C).

Every condition that harbored A83-01 inhibited the presence of mast cells compared with the basal medium S3F11 (Figure 2A, mean % lin-FcεR1α<sup>+</sup> in S3F11-Exp = 22% vs. S3F11+A/AP/AU/APU = 2%,  $p < 0.0001$ ). During mast cell differentiation, S3F11 (and non-A83-01 containing media) cells began to lose the myeloid marker expression in comparison with A83-01-treated cells, which expressed 8–22% more of the myeloid marker CD11b/GR1

(Figure 2B). The abundance of lin<sup>-</sup> cells was largely unaffected by the supplementation of the compounds (Figure 2C).

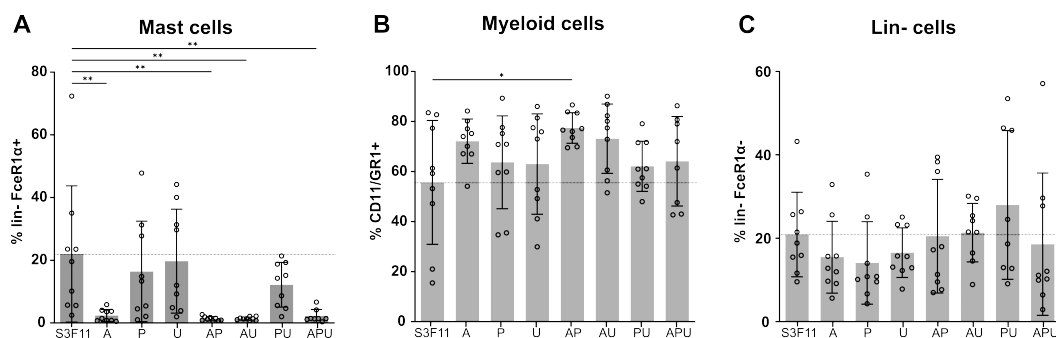


**Figure 2.** A83-01 is the key compound to attenuate mast cell differentiation in S3F11 medium. Surface marker expression after LSK SLAM expansion in S3F11 (ctrl), S3F11+APU, and each single or minus-one compound combination: (A) mast cell (lin-FcεR1α<sup>+</sup>) (B) myeloid (CD11b/GR1<sup>+</sup>) and (C) lin<sup>-</sup> (lin-FcεR1α<sup>-</sup>) marker. Dotted line is equivalent to the mean of the control (S3F11). Significantly fewer mast cells were measured in S3F11+A-containing medium. One-way ANOVA with Dunnett’s multiple comparison was applied to  $n = 3$  experiments each in technical triplicate ( $p > 0.05 = *$ ,  $p < 0.01 = **$ ). All compound conditions were compared with the control medium (S3F11).

### 3.3. Transcriptomic Analysis Confirms the Inhibition of Multiple Differentiation Pathways by A83-01

The transcriptomic signature of S3F11+A83-01-Exp cells was compared with cells expanded in the basal medium (S3F11-Exp). We found 1928 differentially expressed genes after Bonferroni–Holm correction (DEGs;  $p < 0.05$ ,  $|\log_{2}FC| > 1$ ), and the technical replicates clustered according to their medium condition (Figure 3A).

Generally, most DEGs were downregulated by A83-01. In Figure 3B, the volcano plot highlights genes on the outer edges with a potentially high biological relevance due to the consideration of statistical significance [ $-\log(\text{adj.pval})$ ] and magnitude of fold change [ $\log(\text{FC})$ ]. Some of the most significantly downregulated genes by A83-01 were mast cell proteases (*Mcpt4*, *Mcpt2*, *Mcpt1*, *Mcpt9* in order of significance) [39,40], chymases (*Cma1*, *Cma2*) [41,42], tryptases (*Tpsg1*, *Tpsb2*, *Tpsab1*) [43,44], and carboxypeptidases (*Cpa6*, *Cpa3*, *Cpa2*) [45,46]—all enriched in mast cell secretory granules [47]. Additionally, we could confirm a significant reduction of FcεR1α (*FceRa*) in A83-01-treated HSPCs on the transcriptional level (differentially expressed genes are listed in Supplementary Table S2). We performed a gene set enrichment analysis (GSEA) using the M5 gene ontology gene sets from the Mouse Molecular Signatures Database (MSigDB) to identify potential cell type signatures and dysregulated pathways. First, we filtered for expected hematopoietic cell types (“hematopoietic”, “mast\_cell”, “myelo”, “monocyte”, “lymphoid”, “erythro”, “macrophage”, “leuko”, “platelet”, “neutrophil”, “granulocyte”) and TGFβ pathway key words (“transforming\_growth\_factor”, “activin\_receptor”, “smad”, “epithelial\_to\_mesenchymal\_transition”, “MAPK”). The normalized enrichment scores (NES) within the gene ontology sets were plotted against their statistical significance (Figure 3C, all gene ontology pathways in Supplementary Table S3 and filtered pathways with abbreviations in Supplementary Table S4). Most significant gene sets (thrombocytic, myeloid, mast, monocytic, and erythroid cell types) were strongly downregulated in S3F11+A83-01-Exp cells, while only two granulocytic gene sets were significantly enriched. To understand how A83-01 acted on the murine HSPC, we analyzed TGFβ signaling. The ALK5/4/7 inhibitor A83-01 prevents TGFβ signaling by blocking the phosphorylation of Smad2 [14,15]. The phosphorylated Smad2 and Smad3 complex (pSmad2/3) is bound either by TIF1γ to promote erythroid differentiation or by Smad4 to inhibit the proliferation of human HSPCs [48]. On the transcriptional level, we found a significant depletion of gene sets describing TGFβ activation, MAPK cascade, and epithelial-to-mesenchymal transition in

A83-01-treated cultures. Western blot analyses confirmed the absence of pSmad2/3 in S3F11+A/APU-Exp cells, but the presence in S3F11-Exp cells (Figure 4A).

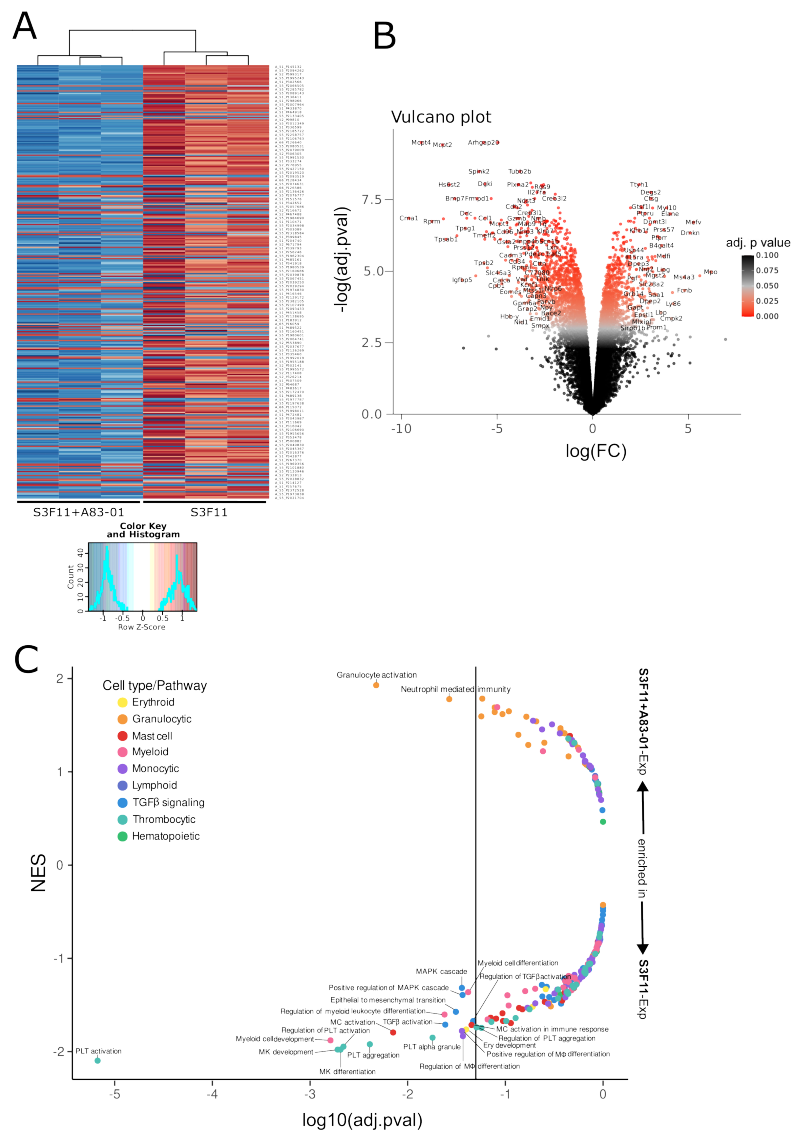


**Figure 3.** Transcriptomic downregulation of several differentiation pathways by A83-01. Transcriptome analysis of S3F11+A83-01-Exp cells versus S3F11-Exp cells with the Agilent Gene Expression Microarray Platform. **(A)** Heat map with hierarchical clustering of all significantly differentially expressed genes ( $p < 0.05$ ) and strong downregulated gene expression in S3F11+A83-01-Exp cells visualized by the negative row Z-score in blue. **(B)** Volcano plot displaying the negative logarithm of the adjusted  $p$ -value [ $-\log(\text{adj.pval.})$ ] against the logarithm of the fold change [ $\log(\text{FC})$ ] in S3F11+A83-01-Exp cells compared with S3F11-Exp. **(C)** Gene set enrichment analysis using the ontology gene sets from the Mouse Molecular Signatures Database (MSigDB) and filtered for cell types and pathways of interest. Normalized enrichment score (NES) is plotted against the decimal logarithm of the adjusted  $p$ -value [ $\log_{10}(\text{adj.pval.})$ ]. Significantly enriched/de-enriched gene sets were labeled in abbreviated form. Positive NES equals an enrichment in S3F11+A83-01-Exp cells, while a negative NES equals an enrichment in S3F11-Exp cells. Thrombocytic-, myeloid-, mast-cell-, monocytic-, erythroid-, and  $\text{TGF}\beta$ -signaling-associated gene sets were significantly downregulated by A83-01.

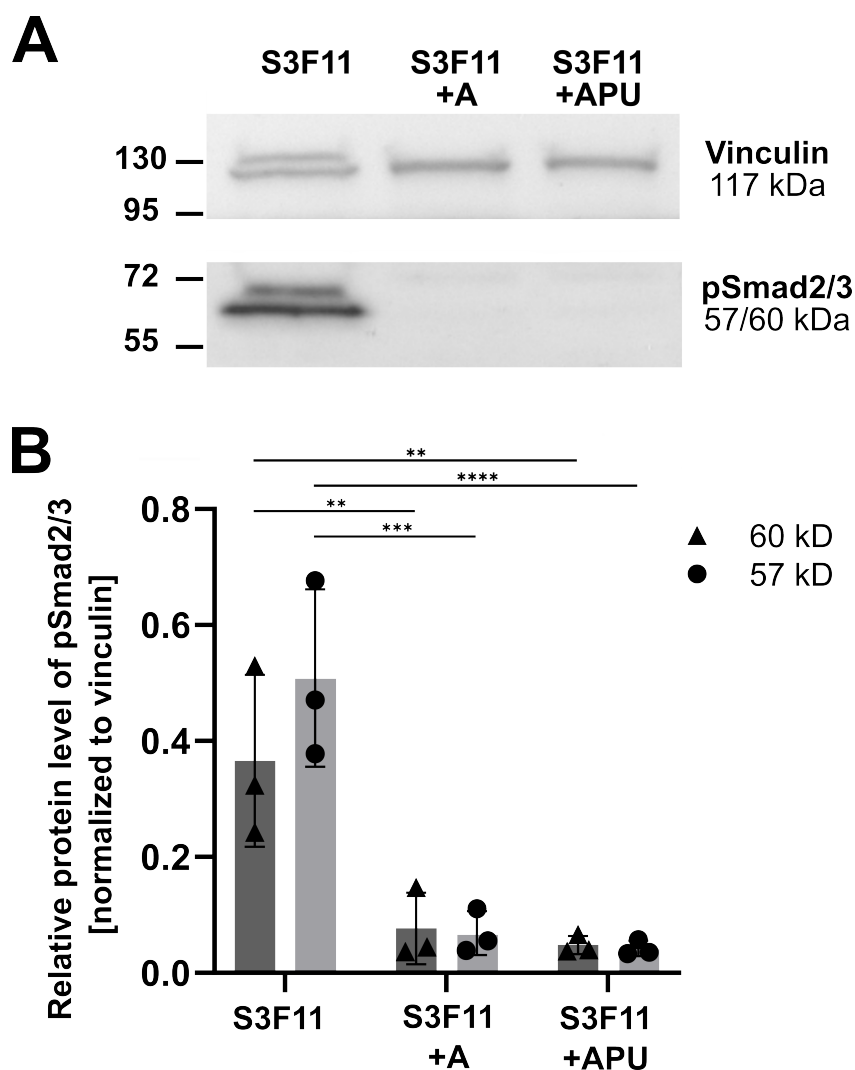


**Figure 4.** A83-01 inhibits pSmad2/3 expression on the protein level. (A) Exemplary Western blot showing the loading control vinculin (117 kDa) and pSmad2/3 (57/60 kDa). Expression of pSmad2/3 is absent in S3F11+A/APU but present in the control S3F11. (B) Densitometric quantification of  $n = 3$  blots. Relative protein level of pSmad2 was calculated by normalizing the density of both pSmad2/3 bands to vinculin. Significant reduction of the pSmad2/3 protein level in S3F11+A/APU. Two-way ANOVA with Dunnett's multiple comparison test was applied to compare A/APU-treated with S3F11 (control),  $p < 0.01 = **$ ,  $p < 0.01 = ***$ ,  $p < 0.0001 = ****$ .

From three experiments, A/APU significantly inhibited pSmad2/3 on the protein level (Figure 4B).

### 3.4. Efficient Transduction of S3F11-APU-Exp Cells for IVIM Assay

If expanded cells shall be used in retroviral vector testing, it is pivotal that they still proliferate after efficient gene modification. In the IVIM assay, transduced and nontransduced mock cultures are cultured for 2 weeks in S3F11 medium (Scheme I). Hence, we transduced cryopreserved expanded cells (S3F11-Exp and S3F11+APU-Exp) and fresh lin-cells (standard material) with a mutagenic gammaretroviral vector (RSF91, Figure 5A) or a safer self-inactivating lentiviral vector with the internal elongation factor 1 alpha short promoter driving transgene expression (EFS, Figure 5A).

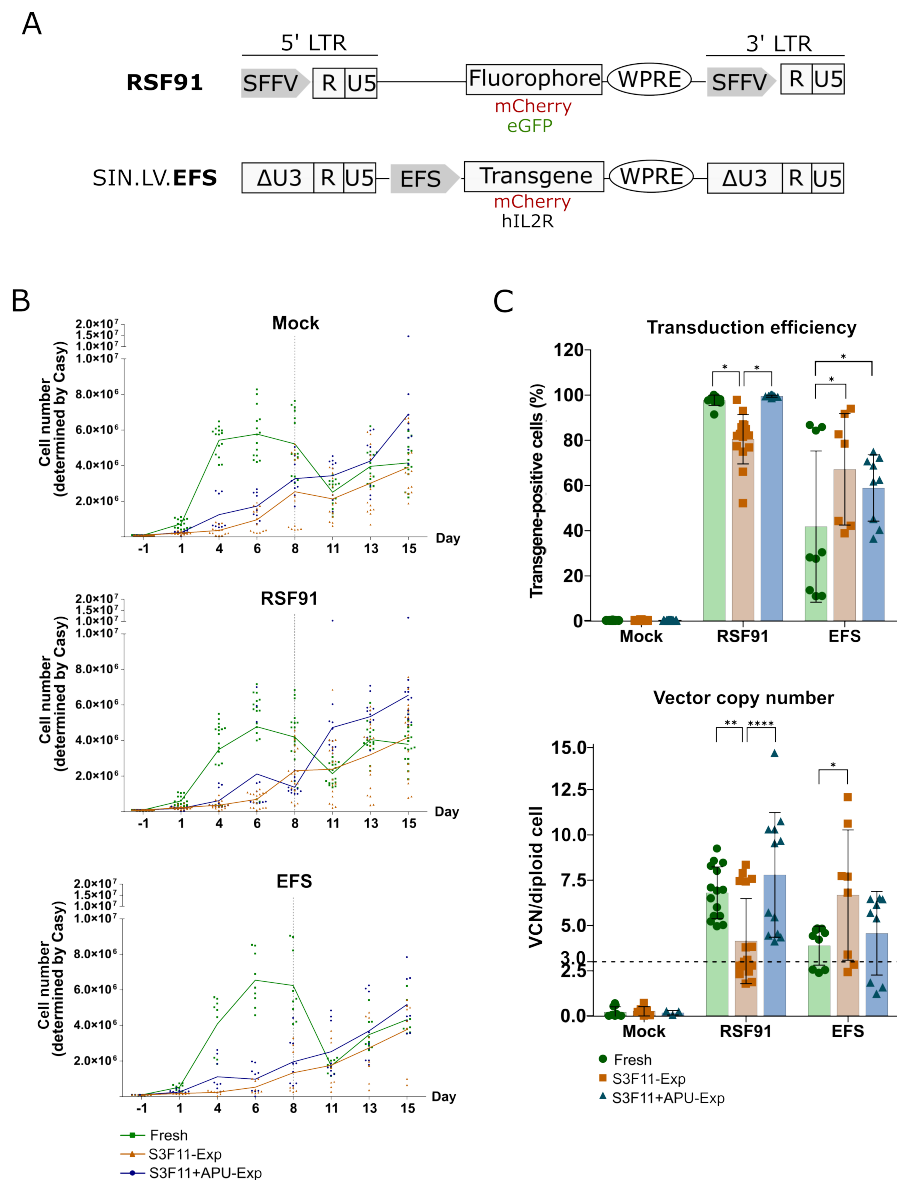


**Figure 5.** Proliferation capacity and transduction efficiency of fresh lin- cells, S3F11-, and S3F11+APU-Exp cells after retroviral transduction for the IVIM assay. **(A)** Cells were modified either with RSF91, an LTR-driven gammaretroviral vector encoding a fluorophore and used as a positive control, or with a self-inactivating lentiviral vector with a transgene (mCherry or hIL2RG) driven by the elongation factor 1 alpha short promoter (SIN.LV.EFS) connected to the anti-silencing CBX3 element1. **(B)** The proliferation of fresh (green), S3F11-Exp (orange), and S3F11+APU-Exp (blue) cells was compared depending on the vector used for transduction: mock, RSF91-, or EFS-transduced. If possible, cells were split on day 8 by seeding  $1 \times 10^6$  cells. Cell numbers were determined by Casy and plotted as individual replicates. The line represents the mean. Fresh cells proliferated strongly after transduction, whereas the expanded cells only recovered after day 8 from the thawing and transduction process. S3F11+APU-Exp cells outperformed both fresh and S3F1-Exp cells by day 15. **(C)** Transduction levels (upper panel) and VCN (lower panel) were determined on day 15 as it was the first time point with a sufficient amount of cells. Transgene-positive cells were determined by flow cytometry. VCN per diploid cell was determined by quantifying the amount of vector-derived WPRE in comparison with genomic PTB2 by Taqman qPCR. The dotted line indicates the minimum VCN of three for the reliable transformation of our positive control. Fresh and S3F11+APU-Exp cells were efficiently transduced with RSF91 in contrast to S3F11-Exp. Statistical analysis performed with two-way ANOVA and Tukey’s multiple comparisons test on  $n = 3$  IVIM assays,  $p < 0.05 = *$ ,  $p < 0.01 = **$ ,  $p < 0.0001 = ****$ .

Before transduction, the immune phenotype of the fresh and expanded material was assessed and compared. In each of the three IVIM assays, the S3F11+APU-Exp cells looked immune phenotypically similar to the fresh lin- cells despite the 2-week-long expansion (Supplementary Figure S1). S3F11-Exp cells were further differentiated than fresh lin- cells. Fresh lin- cells proliferated immediately after thawing and transduction (Figure 5B, green line). In contrast, S3F11-Exp (orange line) and S3F11+APU-Exp (blue line) cells needed time to recover from thawing. However, before replating, S3F11+APU-Exp cells outcompeted fresh cells regarding their proliferation, while S3F11-Exp grew the least and with lower viability in some experiments (Supplementary Figure S2). Transduction efficiency was determined by the level of transgene expression (Figure 5C, upper panel) and the vector integration load (Figure 5C, lower panel). For IVIM, we aim for three RSF91-vector integrations per genome and at least 80% transduction efficiency to elicit immortalization reliably. Flow cytometry revealed highly efficient transduction of fresh lin- and S3F11+APU-Exp cells with RSF91 (>95% transgene positive). On the contrary, S3F11-Exp cells reached significantly lower transduction levels with RSF91, probably due to the lack of cell proliferation, crucial for gammaretroviral vectors for a successful nuclear entry [49,50]. The safer design SIN.LV.EFS exhibited overall lower transduction efficiencies than the gammaretroviral vector. However, our results showed a tendency for both expanded cultures towards higher transduction levels compared with fresh lin- cells, with S3F11-Exp displaying the strongest effect ( $p < 0.05$ ). Fresh lin- and S3F11+APU-Exp cells harbored more than three RSF91-vector copies in all samples per diploid cell, whereas more than half of the S3F11-Exp samples' vector copy number (VCN) was below three. In line with the transgene expression in SIN.LV.EFS-transduced samples, the VCN values in S3F11-Exp cells were significantly higher ( $p < 0.05$ ).

### 3.5. Mutagenic Vector-Induced Differentiation Arrest of Lin- and Myeloid Progenitors in Fresh and S3F11+APU-Exp Cells

To further evaluate expanded cell material for use in genotoxicity assays, we assessed myeloid (CD11b/GR1+), lymphoid/erythroid (CD3/B220/Ter119+), and mast cell (FceR1 $\alpha$ +) differentiation markers by flow cytometry on day 4 (Figure 6A) and day 15 (Figure 6B).

During long-term culture in S3F11, we observed the effect of nonspecific analytical antibody binding by mast cells. Here, we want to highlight the importance of accurate controls to determine specific signals in expansion cultures. Initially, we gated using the fluorescence minus one (FMO) controls. However, when we added the respective isotype control instead of only leaving the specific antibody out, a broad dim false-positive population appeared, especially for anti-CD3/B220/Ter119-APC-Cy7 (Supplementary Figure S3A). We adjusted the gating retrospectively according to the isotype controls (Supplementary Figure S3B). Early cultures (LSK SLAM expansion, day 7) did not harbor any mast cells and thereby no nonspecific binding yet (Supplementary Figure S3C). We could even inhibit this phenomenon in long-term cultures (IVIM, day 29) by incubating the cells with heparin as such false-positive antibody stainings were already described for mast cells on account of their granules (Supplementary Figure S3D) [51,52]. Although fresh lin- cell isolations were cryopreserved with a purity of 70–80%, already on day 4, most cells (>70%) expressed myeloid markers CD11b/GR1+ (Figure 6A, left panel). S3F11+APU-Exp cells had a very similar immune phenotype (>80% CD11b/GR1+) compared with fresh cells (Figure 6A, right panel). In contrast, S3F11-Exp cells expressed only <30% myeloid markers with an increased contribution of mast cells (Figure 6A, middle panel, 40–50% lin-FceR1 $\alpha$ + cells). After 15 days of cultivation in the S3F11 medium, fresh and expanded cultures mostly contained lin-FceR1 $\alpha$ + mast cells (Figure 6B). After 3 weeks of cultivation, virtually all nonimmortalized cultures had only FceR1 $\alpha$ + cells (Figure 6C). Sample RSF91<sub>APU#18</sub> was immortalized (as later shown by the replating step and integration site analysis) and contained a dominant (60%) lin-FceR1 $\alpha$ - population (Figure 6C, right panel). This immune phenotype was accompanied by high proliferation (Supplementary Figure S4). On day 15

post-transduction, cells were replated under limiting dilution to allow the proliferation of potential insertional mutants. However, compared with previously performed IVIM assays (meta-analyses, fresh), the mean replating frequency (RF) of fresh RSF91-transduced samples from the current study was lower than expected. Still, 5 out of 12 replicates scored positive (Supplementary Figure S5, circular dots). When we replated after 22 days of culture instead, the number of positive wells increased to 7 out of 12 (triangle dots). The S3F11-Exp sample RSF91<sub>S3F11#13</sub> (IVIM20210311) showed one immortalized clone after replating on day 21. For APU-Exp cells, only RSF91<sub>APU#18</sub> (IVIM20220311) showed the replating phenotype after day 15 and day 21, but with a higher frequency of positive wells. When expanding clones from the 96-well plate, they were at least 50% negative for lin-markers, <5% FcεR1α+, and expressed only 2–43% myeloid markers. The immortalized clonal phenotype was similar among fresh APU-Exp cells and S3F11-Exp cells (Figure 6D).

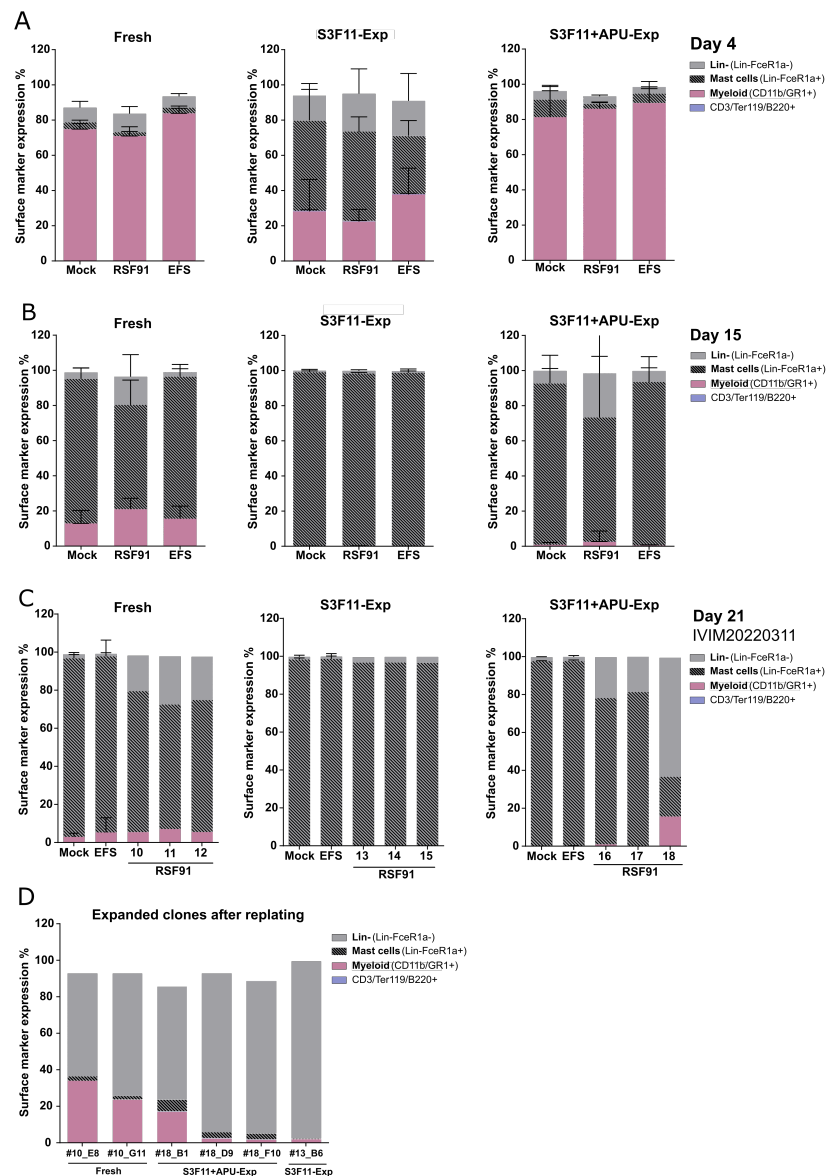


**Figure 6.** Immune phenotypic characterization reveals differentiation arrest of early myeloid progenitors after gammaretroviral transduction. Samples from all three sources were analyzed at different time points by flow cytometry for their surface marker expression. (A) Immune phenotype on day 4

revealed a strong similarity of Fresh and S3F11+APU-Exp cells regarding their composition of lin-, myeloid (CD11b/GR1+), CD3/B220/Ter119+, and mast cell (FcεR1α+) progenitors. S3F11-Exp cells harbored an increased amount of lin-FcεR1α+ cells (n = 3 IVIMs). (B) On day 15, in all three cell sources (Fresh, S3F11-Exp, S2F11+APU-Exp), the bulk culture is mostly lin-FcεR1α+ (n = 3 IVIMs). (C) Single sample analyses from IVIM 20220311 showing the development of individual RSF91-transduced samples in comparison with mock and EFS after 21 days in culture. RSF91-transduced Fresh lin- and S3F11+APU-Exp cells differ from mock and EFS. Sample ID is mentioned below the bars. (D) From positively scored plates, individual wells (labeled below) were picked for the expansion of potential clones in culture. Most clones remained lin-FcεR1α- or CD11b/GR1+.

3.6. Mecom Integrations in Expanded Material Reproduce Clinical Observations and Previous IVIM Results

Immortalized samples (clones) and the respective bulk cultures (day 15) were further characterized for vector integration sites using the integration site pipeline for paired-end reads (INSPIRED) [37,53]. Integrations in or near MECOM were frequently found in patients with severe adverse events (SAE) after gene therapy with retroviral vectors [54–57]. Similarly, vector integrations in or near Mecom are typically found in RSF91-immortalized samples from IVIM/SAGA assays. For the S3F11-Exp and the S3F11+APU-Exp samples with clonal outgrowth on the 96-well plate, INSPIRED detected Mecom as part of the top 10 most abundant insertions in the expanded clones (7.34% contribution for S3F11-Exp, Figure 7A; 20% contribution for S3F11-APU-Exp, Figure 7B).

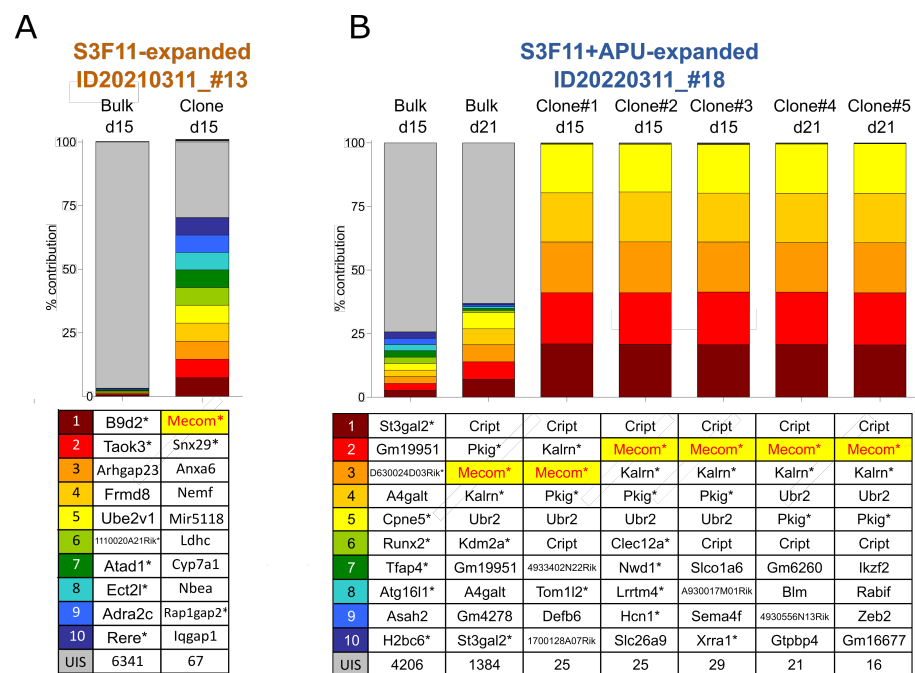
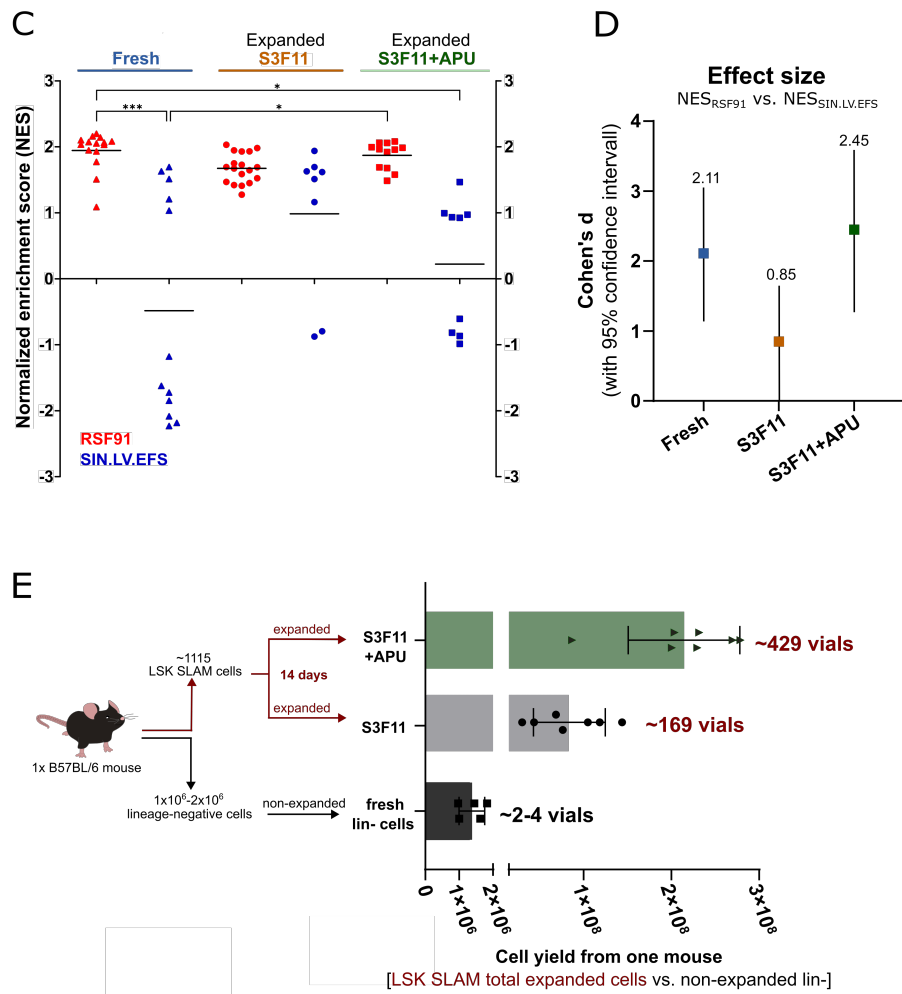


Figure 7. Cont.



**Figure 7.** *Mecom* integration and dysregulated oncogenic gene expression in S3F11 and S3F11+APU-Exp cells after gammaretroviral transduction with RSF91. Integration site analysis with the INSPIRED pipeline and representation of the top 10 most abundant integration sites in (A,B) with highlights on *Mecom* and oncogene (\*) integrations. The count of other unique integration sites (UIS) is described in the last row (gray bar). (A) Integration sites of RSF91-transduced S3F11-Exp bulk population (sample no. 13, IVIM ID 20210311) on day 15 and an expanded clone obtained from low cell density replating. (B) Integration sites of RSF91-transduced S3F11+APU-Exp bulk population (sample no. 18, IVIM ID 20220311) on day 15 and day 21 as well as corresponding expanded clones obtained from both low cell density replating time points. (C) Normalized enrichment score (NES) after gene set enrichment analysis with SAGA (SAGA-GSEA) of APU-expanded (n = 3) and S3F11+APU-Exp (n = 4) IVIM assays using the bulk population from day 15. Statistical analysis performed with one-way ANOVA and Kruskal-Wallis multiple comparisons test,  $p < 0.05 = *$ ,  $p < 0.01 = ***$  (D) Effect size of NES<sub>RSF91</sub> versus NES<sub>SIN.LV.EFS</sub> from SAGA using fresh, S3F11-Exp, or S3F11+APU-Exp cells. Cohen's d of each condition is shown with 95% confidence interval. The biggest effect between RSF91 and SIN.LV.EFS was observed for S3F11+APU-Exp. (E) Cell yield from one mouse after LSK SLAM expansion in S3F11 or S3F11+APU versus after isolating nonexpanded lin- cell for the IVIM assay. Expansion factor of total cell number after 14 days was multiplied by the mean of LSK SLAM cells isolated from one mouse (mean from the last five isolations: 1115 LSK SLAM cells/mouse). Without expansion, one mouse yields cells for only 2–3 IVIM assays ( $5 \times 10^5$ – $1 \times 10^6$  per assay). Expanding LSK SLAM cells in S3F11+APU results in over 400 vials for gene therapy studies.

This dominant insertion, together with the final clonal composition after replating, was not evident at the time of seeding (day 15) for either cell source. Besides *Mecom*, other integrations near or within leukemia-related proto-oncogenes or tumor suppressors were

found within the top 10 most abundant in the expanded clones (*Anxa659* [58], *Nemf* or *Sdcccag1* [59,60], *Ldhc* [61,62], *Nbea* [63], *Rap1gap2* [64,65], *Iqgab1* [66,67], *Cript* [68], *Kalrn* [69], *Pkig* [70,71], and *Ubr2* [72,73]). For the immortalized culture RSF91<sub>APU#18</sub>, INSPIRED detected five integrations in or near *Mecom*, *Cript*, *Kalrn*, *Pkig*, and *Ubr2* with an equal contribution in five clones expanded from the 96-well plate used for replating. This clone with five integrations was also observed when the bulk culture was analyzed after 21 days of cultivation (Figure 7B). The count of unique integration sites (UIS) was highly polyclonal in the bulk samples of day 15 (>4000 UIS) and drastically reduced in the clones (<100 UIS). However, our results suggest that clonal dominance can also be observed in bulk cultures of expanded material after a longer cultivation time.

### 3.7. SAGA Detects an Oncogenic Gene Signature in Expanded Cells after Gammaretroviral Transduction

We previously showed that mutagenic retroviral vectors promote a unique oncogenic gene expression signature compared to mock or safer vector designs that can be used as a more sensitive and reliable alternative than IVIM to predict the genotoxic risk of clinical vectors [30]. SAGA uses a support vector machine (SVM) to classify the samples as transforming based on a core set of eleven predictors. The SAGA bioinformatics pipeline also evaluates the oncogenic signature's enrichment in transduced samples compared with mock with the gene set enrichment analysis (GSEA) tool. From meta-data analyses, we defined a normalized enrichment score (NES) > 1 as a threshold for mutagenicity. The SAGA-GSEA of all three cell sources revealed a mean NES > 1 for RSF91-transduced samples (Figure 7C, red). For the safer SIN.LV.EFS vector, we would expect an NES < 1 as we observed it in our latest meta-data analysis [30]. Indeed, fresh cells resulted in significantly lower NES for the safer vector than RSF91 ( $p < 0.001$ ). Using expanded cells for SIN.LV.EFS transduction slightly enriched the SAGA core set genes (mean NES<sub>fresh</sub> = -0.48 vs. NES<sub>S3F11-Exp</sub> = 0.98; NES<sub>S3F11+APU-Exp</sub> = 0.23). Although there was no significant difference between NES values for SIN.LV.EFS and RSF91 in both expanded conditions, Cohen's d revealed a large effect size between mutagenic and safer vector designs using S3F11+APU-Exp cells, which even outperformed the fresh cells (Figure 7D). When S3F11+APU-Exp were also tested in IVIM and SAGA, they were efficiently transduced (Supplementary Figure S6A) and gave similar SAGA results, likewise S3F11+APU-Exp cells (Supplementary Figure S6B), but no myeloid differentiation block (Supplementary Figure S6C).

For the IVIM assay, we usually require  $5 \times 10^5$ – $1 \times 10^6$  lin<sup>-</sup> cells per experiment. Thus, we isolate lin<sup>-</sup> cells from the BM of a pool of mice and cryopreserve these in  $5 \times 10^5$  lin<sup>-</sup> cells vials. Each mouse harbors around  $1 \times 10^6$  to  $2 \times 10^6$  lin<sup>-</sup> cells, which equal 2–4 vials (Figure 7E). In past experiments, we could isolate between 586 and 1812 LSK SLAM cells per mouse (mean of  $n = 4$  isolations was 1115 cells). If all LSK SLAM cells from one mouse were seeded for expansion in S3F11+APU, we could hypothetically expand them by 201,541-fold (mean expansion factor of total cells shown in Figure 1F) and produce around 449 vials of  $5 \times 10^5$  HSPCs as a homogenous cell product in one huge batch.

Taken together, RSF91-transduced S3F11+APU-Exp cells evidenced arrested cell differentiation of early progenitors, harbored typical high-risk insertions near *Mecom*, and dysregulated specific genes connected to oncogenesis. The similar behavior of this S3F11+APU-Exp material to fresh cells makes it potentially suitable for genotoxicity assays and thereby reduces the number of experimental mice needed, according to the 3R principles.

## 4. Discussion

Ex vivo HSPC cultivation is currently unavoidable for the retroviral gene correction of HSPCs. In gene therapeutic protocols, IL-3 is part of various transduction and expansion media to promote proliferation [74–77]. In our study, media containing IL-3 and other cytokines essential for stem cell expansion (S3F11) massively expanded myeloid progenitors, which, however, unfortunately, rapidly differentiated into mast cells. We aimed to attenuate such myeloid differentiation to enable the use of expanded cells for genotoxicity studies.

By intervening in the phosphorylation of Smad2 with the small compound A83-01 [15], myeloid differentiation, specifically to mast cells, was inhibited while we could expand lin-cKit<sup>+</sup> hematopoietic progenitors over 20,000-fold and LSK cells around 3800-fold.

TGF $\beta$  signaling determines self-renewal or differentiation in HSCs. High concentrations of TGF $\beta$  can be found in the bone marrow niche and restrict the cycling of HSCs [78–80], while low concentrations promote the expansion of myeloid progenitors [28,81]. In other studies, the activation of “quiescent” cells was observed when neutralizing antibodies against TGF $\beta$  were combined with myeloid cytokines, such as IL-3 and IL-6. The combinatorial approach increased the number of colony-forming units and the long-term repopulating capacity of HSPCs compared with cells exposed to TGF $\beta$  [82,83]. We could observe similar beneficial effects of using the TGF $\beta$  inhibitor A83-01 in our S3F11 basal medium for HSPC expansion. However, although the single and minus-one experiments and the microarray analysis suggested that A83-01 is the main effector, we cannot entirely exclude synergistic effects with the other compounds (pomalidomide and UM171).

The HSPC expansion effect of TGF $\beta$  inhibition could be of interest for the gene therapy of Fanconi anemia (FA) patients. Due to the BM failure in FA, isolating sufficient cell numbers for gene correction can be challenging [84]. In an ongoing clinical trial (ClinicalTrials.gov, NCT03157804; European Clinical Trials Database, 2011-006100-12), the efficacy of gene correction was proven, but only patients transplanted with higher numbers of transduced CD34<sup>+</sup> cells showed substantial hematopoietic reconstitution [85]. The ex vivo expansion of HSPCs might lead to more polyclonal repopulation after gene therapy. Furthermore, TGF $\beta$  signaling is described to be overexpressed in FA patients. This effect might contribute to the dysfunctionality of HSPCs in FA patient BM [86]. TGF $\beta$  inhibitors were tested as an alternative therapy to combat HSC exhaustion [87] but not combined with a gene therapeutic approach so far.

S3F11+APU-Exp cells could be transduced as efficiently as fresh BM lin<sup>-</sup> cells. The similar immune phenotype of fresh and S3F11+APU-Exp cells on the day of transduction suggests that early progenitors and potentially true transplantable HSCs can be transduced. Although we did not perform transplantation studies with the expanded mouse material, we are currently adapting the protocol for use with human umbilical cord blood-derived HSPCs to analyze the effects of expansion on engraftment. Xenotransplantation studies with a clinically relevant cell type will shed further light on the applicability of TGF $\beta$  inhibition in transduction protocols and, ultimately, hematopoietic stem cell transplantation.

Preclinical safety studies, including genotoxicity testing, of novel integrating vectors for gene therapy are mandatory [88,89]. We have previously developed the genotoxicity assays IVIM and SAGA to assess the risk of insertional mutagenesis by retroviral vectors [29,30]. Both assays constantly require murine BM-derived lin<sup>-</sup> cells. In this study, we propose using expanded cells to reduce the number of experimental animals while maintaining the quality of the assays. The IVIM assay focuses on the proliferation of transformed cells at very low cell densities. The immune phenotype of immortalized clones was not characterized in detail until now. Here, we presented a promising positive genotoxic readout in the form of a myeloid differentiation block in fresh lin<sup>-</sup> and S3F11+APU-Exp cells transduced with the mutagenic RSF91 vector. The absence of Fc $\epsilon$ R1 $\alpha$  and a lin<sup>-</sup> marker but an expression of early myeloid marker GR1/CD11b predicted transformation prior to replating in limiting dilution. This shortened the assay duration by 1 to 2 weeks. Mock and SIN.LV.EFS-transduced cells did not show the differentiation block. However, we observed a decreased incidence of immortalized clones compared with the meta-analysis of the past decades. We could only observe one clear transformation in three assays using S3F11+APU-Exp, and so far, none in the two assays using S3F11+A-Exp cells. Hence, the sensitivity of IVIM with expanded cells might be reduced compared with fresh cell material. So far, we cannot say which progenitor type is required for immortalization. It is likely that fresh lin<sup>-</sup> cells and expanded LSK SLAM cells contain different progenitors. APU promoted the expansion of multipotent progenitors (MPPs). When the cells are used in the IVIM

assay, the frequency of MPPs could influence the rate of vector-induced immortalization. Since insertional mutagenesis requires proliferative pressure to allow the development of clonal dominance, postponing the replating for 1 week increased the number of positively scored wells and even only allowed the development of one clone in IVIM20210311 with S3F11-Exp after longer culture before replating. In long-term monitoring trials, adverse events can occur years after gene correction, which is unfeasible to recapitulate in a cell culture system. Therefore, the detection of vector integration sites and the use of more sensitive assays based on transcriptional dysregulation add necessary measures for reliable prediction of genotoxicity.

*Mecom* is transcribed in HSCs and encodes for transcription factors regulating their proliferation, long-term repopulating capacity, and self-renewal [90–93]. All transformed clones in our experiments with expanded material harbored an integration in or near *Mecom*. Typically, vector integrations near *Mecom* are responsible for insertional mutagenesis in IVIM/SAGA due to the overexpression of the transcription factors promoting proliferation, as seen in leukemia (reviewed here [94]). Clones derived from RSF91<sub>APU#18</sub> culture had five codominant insertions per cell. We did not observe any clonal dominance on day 15, and on day 21, the abundance of each dominant integration was <10%. When patients in gene therapy trials are monitored, the abundance of individual integrations above a certain threshold (previously 30% or now often 10%) can elicit closer monitoring intervals. Where a single integration did not contribute more than 10% in our in vitro example, the combination of the five integrations contributed over 25%. Such examples highlight the immense awareness required for monitoring high-risk insertion sites and the diversity of clonal patterns contributing to clinical trial decision processes.

SAGA unfailingly classified RSF91-transduced samples as mutagenic due to the enrichment in stemness- and cancer-associated genes, regardless of the cell source used in this study. The large effect size of NES<sub>RSF91</sub> compared with NES<sub>SIN.LV.EFS</sub> confirmed the clear distinction between mutagenic and the safer vector in fresh and even higher in S3F11+APU-Exp cells. Although the machine learning process for SAGA was developed with fresh cells, we could apply the readout to S3F11+APU-Exp cells. The NES<sub>SIN.LV.EFS</sub> of S3F11+APU-Exp cells even overlapped less with NES<sub>RSF91</sub>, which resulted in a higher effect size. However, the lowest NES<sub>SIN.LV.EFS</sub> of the fresh samples was classified around  $-2$  compared with the expanded samples, which only reached a minimum NES of around  $-1$ , resulting in a lower mean for the fresh samples. Potentially, the background of cells transduced with a safer lentiviral vector could be higher in S3F11+APU-Exp cells since we did not see signs of transformation on the immune phenotypical level in these samples. S3F11-Exp cells gave the least clear result, likely due to the further progressed differentiation before transduction. On day 15 of IVIM, this could have resulted in a transcriptomic signature too different from the SAGA signature set using fresh cells. The development of the SAGA pipeline used over 160 data points to determine a reliable set of genotoxicity predictors. A similar number of data points would have to be gathered with expanded cell material over time to reach a similar performance. Nevertheless, SAGA's ability to predict transformation confirmingly showed a higher sensitivity than the IVIM assay.

So far, reliable human hematopoietic genotoxicity assays are missing. The transduction and long-term maintenance of human CD34+ HPSCs is challenging. For our positive control, the gammaretroviral vector RSF91, cell division is crucial for vector integration [49,95,96]. Hence, low cycling of HSPCs limits the high transduction efficiency needed for a positive genotoxic readout. We could not achieve desired transduction levels in CD34+ cells using well-known small compounds for HSPC expansion, StemRegenin-1 or UM171 [25,27]. Thus, we are currently testing the APU compounds to expand human umbilical cord blood-derived HSPCs for a humanized version of the IVIM assay. Characterizing a transforming immune phenotype and dysregulated transcriptional pattern after retroviral transduction could establish a genotoxic readout on transduced patient material before transplantation.

## 5. Conclusions

This study proposes using A83-01 to inhibit mast cell differentiation for mouse HSPC cultured in the presence of IL-3. A83-01 blocked the phosphorylation of Smad2 and led to a 20,000-fold expansion of lin-ckit+ cells and a 3800-fold expansion of LSK cells. Expanded progenitors were transduced efficiently with gamma- and lentiviral vectors comparable to uncultivated lin- cells. We tested their functionality in the preclinical biosafety assays IVIM and SAGA. Expanded HSPCs could immortalize after transduction with a mutagenic vector due to virus integration nearby Mecom, however, with an overall lower incidence than fresh lin- cells. More replicates are required to validate the use of expanded HP-SCs in genotoxicity assays, which would reduce the number of experimental animals by 200–400-fold due to the immense expansion potential LSK SLAM cells have in S3F11+A83-01 or +APU medium.

**Supplementary Materials:** The following supporting information can be downloaded at: <https://www.mdpi.com/article/10.3390/cells12151978/s1>, Table S1: Expansion media composition; Table S2: Significantly differentially expressed genes in S3F11+A83-01; Table S3: M5 ontology gene sets from the GSEA Mouse MSigDB Collections; Table S4: Filtered M5 ontology gene sets from the GSEA Mouse MSigDB Collections; Figure S1: Surface marker expression of three individual IVIMs on day –1; Figure S2: Viability of fresh and expanded cells in the IVIM assay on day 11; Figure S3: Non-specific binding in long-term cultures by mast cells; Figure S4: Proliferation curves from IVIM 20220311 of fresh, S3F11-Exp and S3F11+APU-Exp cells; Figure S5: Replating frequency (RF) of individual IVIM samples based on the number of positively scored wells after replating either on day 15 (circle) or day 22 (triangle); Figure S6: IVIM and SAGA using S3F11+A-Exp cells. References [13,29,97,98] are cited in the supplementary materials.

**Author Contributions:** Conceptualization, J.F., M.R. and A.S. (Axel Schambach); data curation, J.F., M.R. and P.J.-N.; formal analysis, J.F., A.L.B. and P.J.-N.; funding acquisition, M.R. and A.S. (Axel Schambach); investigation, J.F., A.L.B., D.S., L.W. and D.S.; methodology, J.F. and M.R.; project administration, J.F., M.R. and A.S. (Axel Schambach); resources, M.R. and A.S. (Axel Schambach); supervision, M.R., A.S. (Axel Schambach) and A.S. (Anton Selich); validation, J.F., M.R., A.S. (Axel Schambach) and A.S. (Anton Selich); visualization, J.F. and P.J.-N.; writing—original draft, J.F.; writing—review and editing, J.F., A.L.B., A.S. (Anton Selich) and M.R. All authors have read and agreed to the published version of the manuscript.

**Funding:** This research was funded by the German Research Foundation (Deutsche Forschungsgemeinschaft, DFG) RO 5102/1-2 and the Federal State of Lower Saxony (research project R2N). Results incorporated in this study received funding from the European Union Horizon 2020 Research and Innovation Program (755170).

**Institutional Review Board Statement:** Isolation of animal cells was approved by the Institutional Review Board of the Institute for Laboratory Animal Science, Hannover Medical School, Hannover, Germany (No. 2020-254).

**Informed Consent Statement:** Not applicable.

**Data Availability Statement:** Not applicable.

**Acknowledgments:** We gratefully acknowledge the help for the Western blot experiments from our colleague Larissa Nassauer, Institute of Experimental Hematology, Hannover Medical School, and Sarah Cushman and Arne Schmidt, IMTTS, Hannover Medical School, for providing the anti-vinculin antibody. We thank Matthias Ballmaier in the flow cytometry core unit of the Hannover Medical School for performing the cell sorting experiments.

**Conflicts of Interest:** The authors declare no conflict of interest.

## Abbreviations

The following abbreviations are used in this manuscript:

HSPCs	hematopoietic stem and progenitor cells
BM	bone marrow
APU	A83-01, pomalidomide, UM171
lin-	lineage-negative
LSK SLAM	lin- Sca1+ cKit+ CD48- CD150+
SCF	stem cell factor
IL	interleukin
FLT3-L	FMS-like tyrosine kinase 3 ligand
HSCs	hematopoietic stem cells
FcεR1α	Fc epsilon receptor 1 alpha
S3F11	SCF, IL-3, FLT3-L, IL-11
TPO	thrombopoietin
ALK	activin receptor-like kinase
CRL4 <sup>CRBN</sup>	CUL4-RBX1-DDB1-CRBN
IVIM assay	in vitro immortalization assay
SAGA	surrogate assay for genotoxicity
Exp	expanded
Mecom	MDS1 and EVI1 complex locus
EDTA	ethylenediaminetetraacetic acid
FACS	Fluorescent-activated cell sorting
FCS	fetal calf serum
MTT	thiazolyl blue tetrazolium bromide
SDS	sodium dodecyl sulfate
RT	room temperature
VCN	vector copy number
WPRE	woodchuck hepatitis virus post-transcriptional regulatory element
PTBP2	polypyrimidine tract binding protein 2
NES	normalized enrichment score
INSPIRED	integration site pipeline for paired-end reads
STIF	SCF, TPO, IGF2, FGF1
IGF2	insulin-like growth factor 2
FGF1	fibroblast growth factor 1
DEG	differentially expressed genes
GSEA	gene set enrichment analysis
MSigDB	Mouse Molecular Signatures Database
RF	replating frequency
UIS	unique integration sites
SVM	support vector machine
FA	Fanconi Anemia

## References

1. Meyts, I.; Bousfiha, A.; Duff, C.; Singh, S.; Lau, Y.L.; Condino-Neto, A.; Bezrodnik, L.; Ali, A.; Adeli, M.; Drabwell, J. Primary Immunodeficiencies: A Decade of Progress and a Promising Future. *Front. Immunol.* **2021**, *11*, 625753. [[CrossRef](#)] [[PubMed](#)]
2. Notarangelo, L.D. Primary immunodeficiencies. *J. Allergy Clin. Immunol.* **2010**, *125*, S182–S194. [[CrossRef](#)]
3. Taher, A.T.; Weatherall, D.J.; Cappellini, M.D. Thalassaemia. *Lancet* **2018**, *391*, 155–167. [[CrossRef](#)] [[PubMed](#)]
4. Scalone, L.; Mantovani, L.G.; Krol, M.; Rofail, D.; Ravera, S.; Grazia Bisconte, M.; Borgna-Pignatti, C.; Borsellino, Z.; Cianciulli, P.; Gallisai, D.; et al. Costs, quality of life, treatment satisfaction and compliance in patients with  $\beta$ -thalassaemia major undergoing iron chelation therapy: the ITHACA study. *Curr. Med. Res. Opin.* **2008**, *24*, 1905–1917. [[CrossRef](#)] [[PubMed](#)]
5. Kohne, E. Hämoglobinopathien: Klinische erscheinungsbilder, diagnostische und therapeutische hinweise. *Dtsch. Ärztebl. Int.* **2011**, *108*, 532. [[CrossRef](#)]
6. Dokal, I.; Vulliamy, T. Inherited aplastic anaemias/bone marrow failure syndromes. *Blood Rev.* **2008**, *22*, 141–153. [[CrossRef](#)]
7. Dokal, I.; Vulliamy, T. Inherited bone marrow failure syndromes. *Haematologica* **2010**, *95*, 1236. [[CrossRef](#)]
8. Shimamura, A.; Alter, B.P. Pathophysiology and management of inherited bone marrow failure syndromes. *Blood Rev.* **2010**, *24*, 101–122. [[CrossRef](#)]

9. Ballabio, A.; Gieselmann, V. Lysosomal disorders: From storage to cellular damage. *Biochim. Biophys. Acta-Mol. Cell Res.* **2009**, *1793*, 684–696. [[CrossRef](#)]
10. Platt, F.M.; D’Azzo, A.; Davidson, B.L.; Neufeld, E.F.; Tifft, C.J. Lysosomal storage diseases. *Nat. Rev. Dis. Prim.* **2018**, *4*, 27. [[CrossRef](#)]
11. Lui, W.C.; Chan, Y.F.; Chan, L.C.; Ng, R.K. Cytokine combinations on the potential for ex vivo expansion of murine hematopoietic stem cells. *Cytokine* **2014**, *68*, 127–132. [[CrossRef](#)]
12. Nitsche, A.; Junghahn, I.; Thulke, S.; Aumann, J.; Radoni, A.; Fichtner, I.; Siegert, W.; Radonic, A. Interleukin-3 Promotes Proliferation and Differentiation of Human Hematopoietic Stem Cells but Reduces Their Repopulation Potential in NOD/SCID Mice. *Stem Cells* **2003**, *21*, 236–244. [[CrossRef](#)]
13. Ebina, W. Combinatorial Pathway Modulation toward Ex Vivo Maintenance and Propagation of Hematopoietic Stem Cells. Ph.D. Thesis, Harvard University, Cambridge, MA, USA, 2016.
14. Li, W.; Wei, W.; Zhu, S.; Zhu, J.; Shi, Y.; Lin, T.; Hao, E.; Hayek, A.; Deng, H.; Ding, S. Generation of Rat and Human Induced Pluripotent Stem Cells by Combining Genetic Reprogramming and Chemical Inhibitors. *Cell Stem Cell* **2009**, *4*, 16–19. [[CrossRef](#)]
15. Tojo, M.; Hamashima, Y.; Hanyu, A.; Kajimoto, T.; Saitoh, M.; Miyazono, K.; Node, M.; Imamura, T. The ALK-5 inhibitor A-83-01 inhibits Smad signaling and epithelial-to-mesenchymal transition by transforming growth factor- $\beta$ . *Cancer Sci.* **2005**, *96*, 791–800. [[CrossRef](#)]
16. Batard, P.; Monier, M.N.; Fortunel, N.; Ducos, K.; Sansilvestri-Morel, P.; Phan, T.H.; Hatzfeld, A.; Hatzfeld, J.A. TGF- $\beta$ 1 maintains hematopoietic immaturity by a reversible negative control of cell cycle and induces CD34 antigen up-modulation. *J. Cell Sci.* **2000**, *113*, 383–390. [[CrossRef](#)]
17. Sitnicka, E.; Ruscetti, F.W.; Priestley, G.V.; Wolf, N.S.; Bartelmez, S.H. Transforming growth factor  $\beta$ 1 directly and reversibly inhibits the initial cell divisions of long-term repopulating hematopoietic stem cells. *Blood* **1996**, *88*, 82–88. [[CrossRef](#)]
18. Pajcini, K.V.; Speck, N.A.; Pear, W.S. Notch signaling in mammalian hematopoietic stem cells. *Leukemia* **2011**, *25*, 1525–1532. [[CrossRef](#)] [[PubMed](#)]
19. Lamprea, F.P.; Carmelo, J.G.; Anjos-Afonso, F. Notch Signaling in the Regulation of Hematopoietic Stem Cell. *Curr. Stem Cell Rep.* **2017**, *3*, 202–209. [[CrossRef](#)] [[PubMed](#)]
20. Kleinmann, E.; Geimer Le Lay, A.S.; Sellars, M.; Kastner, P.; Chan, S. Ikaros Represses the Transcriptional Response to Notch Signaling in T-Cell Development. *Mol. Cell. Biol.* **2008**, *28*, 7465–7475. [[CrossRef](#)] [[PubMed](#)]
21. Kathrein, K.L.; Chari, S.; Winandy, S. Ikaros directly represses the notch target gene Hes1 in a leukemia T cell line: Implications for CD4 regulation. *J. Biol. Chem.* **2008**, *283*, 10476–10484. [[CrossRef](#)] [[PubMed](#)]
22. Witkowski, M.T.; Cimmino, L.; Hu, Y.; Trimarchi, T.; Tagoh, H.; McKenzie, M.D.; Best, S.A.; Tuohey, L.; Willson, T.A.; Nutt, S.L.; et al. Activated Notch counteracts Ikaros tumor suppression in mouse and human T-cell acute lymphoblastic leukemia. *Leukemia* **2015**, *29*, 1301–1311. [[CrossRef](#)]
23. Fischer, E.S.; Böhm, K.; Lydeard, J.R.; Yang, H.; Stadler, M.B.; Cavadini, S.; Nagel, J.; Serluca, F.; Acker, V.; Lingaraju, G.M.; et al. Structure of the DDB1-CRBN E3 ubiquitin ligase in complex with thalidomide. *Nature* **2014**, *512*, 49–53. [[CrossRef](#)]
24. Petzold, G.; Fischer, E.S.; Thomä, N.H. Structural basis of lenalidomide-induced CK1 $\alpha$  degradation by the CRL4 CRBN ubiquitin ligase. *Nature* **2016**, *532*, 127–130. [[CrossRef](#)]
25. Boitano, A.E.; Wang, J.; Romeo, R.; Bouchez, L.C.; Parker, A.E.; Sutton, S.E.; Walker, J.R.; Flaveny, C.A.; Perdew, G.H.; Denison, M.S.; et al. Aryl Hydrocarbon Receptor Antagonists Promote the Expansion of Human Hematopoietic Stem Cells. *Science* **2010**, *329*, 1345–1348. [[CrossRef](#)]
26. Chagraoui, J.; Girard, S.; Spinella, J.F.; Simon, L.; Bonneil, E.; Mayotte, N.; MacRae, T.; Coulombe-Huntington, J.; Bertomeu, T.; Moison, C.; et al. UM171 Preserves Epigenetic Marks that Are Reduced in Ex Vivo Culture of Human HSCs via Potentiation of the CLR3-KBTBD4 Complex. *Cell Stem Cell* **2021**, *28*, 48–62. [[CrossRef](#)]
27. Cohen, S.; Roy, J.; Lachance, S.; Delisle, J.S.; Marinier, A.; Busque, L.; Roy, D.C.; Barabé, F.; Ahmad, I.; Bambace, N.; et al. Hematopoietic stem cell transplantation using single UM171-expanded cord blood: A single-arm, phase 1-2 safety and feasibility study. *Lancet Haematol.* **2019**, *7*, e134–e145. [[CrossRef](#)] [[PubMed](#)]
28. Blank, U.; Karlsson, S. TGF- $\beta$  signaling in the control of hematopoietic stem cells. *Blood J. Am. Soc. Hematol.* **2015**, *125*, 3542–3550. [[CrossRef](#)]
29. Modlich, U.; Bohne, J.; Schmidt, M.; Von Kalle, C.; Knöss, S.; Schambach, A.; Baum, C. Cell-culture assays reveal the importance of retroviral vector design for insertional genotoxicity. *Blood* **2006**, *108*, 2545–2553. [[CrossRef](#)]
30. Schwarzer, A.; Talbot, S.R.; Selich, A.; Morgan, M.; Schott, J.W.; Dittrich-Breiholz, O.; Bastone, A.L.; Weigel, B.; Ha, T.C.; Dziadek, V.; et al. Predicting genotoxicity of viral vectors for stem cell gene therapy using gene expression-based machine learning. *Mol. Ther.* **2021**, *29*, 3383–3397. [[CrossRef](#)] [[PubMed](#)]
31. Schambach, A.; Wodrich, H.; Hildinger, M.; Bohne, J.; Kräusslich, H.G.; Baum, C. Context dependence of different modules for posttranscriptional enhancement of gene expression from retroviral vectors. *Mol. Ther.* **2000**, *2*, 435–445. [[CrossRef](#)] [[PubMed](#)]
32. Schambach, A.; Mueller, D.; Galla, M.; Versteegen, M.M.; Wagemaker, G.; Loew, R.; Baum, C.; Bohne, J. Overcoming promoter competition in packaging cells improves production of self-inactivating retroviral vectors. *Gene Ther.* **2006**, *13*, 1524–1533. [[CrossRef](#)] [[PubMed](#)]
33. Hildinger, M.; Abel, K.L.; Ostertag, W.; Baum, C. Design of 5’ Untranslated Sequences in Retroviral Vectors Developed for Medical Use. *J. Virol.* **1999**, *73*, 4083–4089. [[CrossRef](#)]

34. Schambach, A.; Bohne, J.; Chandra, S.; Will, E.; Margison, G.P.; Williams, D.A.; Baum, C. Equal potency of gammaretroviral and lentiviral SIN vectors for expression of O6-methylguanine-DNA methyltransferase in hematopoietic cells. *Mol. Ther.* **2006**, *13*, 391–400. [[CrossRef](#)] [[PubMed](#)]
35. Zufferey, R.; Dull, T.; Mandel, R.J.; Bukovsky, A.; Quiroz, D.; Naldini, L.; Trono, D. Self-inactivating lentivirus vector for safe and efficient in vivo gene delivery. *J. Virol.* **1998**, *72*, 9873–9880. [[CrossRef](#)]
36. Schwarzer, A.; Talbot, S.R.; Dittrich-Breiholz, O.; Thrasher, A.J.; Gaspar, B.; Modlich, U.; Baum, C.; Schambach, A.; Rothe, M. New Molecular Surrogate Assay for Genotoxicity Assessment of Gene Therapy Vectors (SAGA). *Blood* **2016**, *128*, 4710. [[CrossRef](#)]
37. Berry, C.C.; Nobles, C.; Six, E.; Wu, Y.; Malani, N.; Sherman, E.; Dryga, A.; Everett, J.K.; Male, F.; Bailey, A.; et al. INSPIRED: Quantification and Visualization Tools for Analyzing Integration Site Distributions. *Mol. Ther.-Methods Clin. Dev.* **2017**, *4*, 17–26. [[CrossRef](#)] [[PubMed](#)]
38. Wilkinson, A.C.; Ishida, R.; Kikuchi, M.; Sudo, K.; Morita, M.; Crisostomo, R.V.; Yamamoto, R.; Loh, K.M.; Nakamura, Y.; Watanabe, M.; et al. Long-term ex vivo haematopoietic-stem-cell expansion allows nonconditioned transplantation. *Nature* **2019**, *571*, 117–121. [[CrossRef](#)]
39. Pejler, G.; Rönnberg, E.; Waern, I.; Wernersson, S. Mast cell proteases: Multifaceted regulators of inflammatory disease. *Blood J. Am. Soc. Hematol.* **2010**, *115*, 4981–4990. [[CrossRef](#)]
40. Dai, H.; Korthuis, R.J. Mast cell proteases and inflammation. *Drug Discov. Today Dis. Model.* **2011**, *8*, 47–55. [[CrossRef](#)]
41. Benditt, E.P.; Arase, M. An enzyme in mast cells with properties like chymotrypsin. *J. Exp. Med.* **1959**, *110*, 451–460. [[CrossRef](#)]
42. Pejler, G. Novel Insight into the in vivo Function of Mast Cell Chymase: Lessons from Knockouts and Inhibitors. *J. Innate Immun.* **2020**, *12*, 357–372. [[CrossRef](#)]
43. Glenner, G.G.; Cohen, L.A. Histochemical demonstration of a species-specific trypsin-like enzyme in mast cells. *Nature* **1960**, *185*, 846–847. [[CrossRef](#)]
44. Schwartz, L.B.; Metcalfe, D.D.; Miller, J.S.; Earl, H.; Sullivan, T. Tryptase Levels as an Indicator of Mast-Cell Activation in Systemic Anaphylaxis and Mastocytosis. *N. Engl. J. Med.* **1987**, *316*, 1622–1626. [[CrossRef](#)] [[PubMed](#)]
45. Atiakshin, D.; Kostin, A.; Trotsenko, I.; Samoilova, V.; Buchwalow, I.; Tiemann, M. Carboxypeptidase A3-A Key Component of the Protease Phenotype of Mast Cells. *Cells* **2022**, *11*, 570. [[CrossRef](#)]
46. Ahmada, S.; Wrighta, K.N.; Sunb, X.; Grobanb, L.; Ferrarioa, C.M. Mast cell peptidases (carboxypeptidase A and chymase)-mediated hydrolysis of human angiotensin-(1–12) substrate Sarfaraz. *Biochem. Biophys. Res. Commun.* **2019**, *176*, 139–148. [[CrossRef](#)]
47. Wernersson, S.; Pejler, G. Mast cell secretory granules: Armed for battle. *Nat. Publ. Group* **2014**, *14*, 478–494. [[CrossRef](#)]
48. He, W.; Dorn, D.C.; Erdjument-Bromage, H.; Tempst, P.; Moore, M.A.; Massagué, J. Hematopoiesis Controlled by Distinct TIF1 $\gamma$  and Smad4 Branches of the TGF $\beta$  Pathway. *Cell* **2006**, *125*, 929–941. [[CrossRef](#)] [[PubMed](#)]
49. Lewis, P.F.; Emerman, M. Passage through mitosis is required for oncoretroviruses but not for the human immunodeficiency virus. *J. Virol.* **1994**, *68*, 510–516. [[CrossRef](#)]
50. Miller, D.G.; Adam, M.A.; Miller, A.D. Gene Transfer by Retrovirus Vectors Occurs Only in Cells That Are Actively Replicating at the Time of Infection. *Mol. Cell. Biol.* **1990**, *10*, 4239–4242.
51. Ruck, P.; Horny, H.P.; Kaiserling, E. Immunoreactivity of human tissue mast cells: Nonspecific binding of primary antibodies against regulatory peptides by ionic linkage. *J. Histochem. Cytochem.* **1990**, *38*, 859–867. [[CrossRef](#)] [[PubMed](#)]
52. Schiltz, P.M.; Lieber, J.; Giorno, R.C.; Claman, H.N. Mast cell immunohistochemistry: Non-immunological immunostaining mediated by non-specific F(ab')<sub>2</sub>-mast cell secretory granule interaction. *Histochem. J.* **1993**, *25*, 642–647. [[CrossRef](#)]
53. Sherman, E.; Nobles, C.; Berry, C.C.; Six, E.; Wu, Y.; Dryga, A.; Malani, N.; Male, F.; Reddy, S.; Bailey, A.; et al. INSPIRED: A Pipeline for Quantitative Analysis of Sites of New DNA Integration in Cellular Genomes. *Mol. Ther.-Methods Clin. Dev.* **2017**, *4*, 39–49. [[CrossRef](#)]
54. Stein, S.; Ott, M.G.; Schultze-Strasser, S.; Jauch, A.; Burwinkel, B.; Kinner, A.; Schmidt, M.; Krämer, A.; Schwäble, J.; Glimm, H.; et al. Genomic instability and myelodysplasia with monosomy 7 consequent to EVI1 activation after gene therapy for chronic granulomatous disease. *Nat. Med.* **2010**, *16*, 198–204. [[CrossRef](#)]
55. Métais, J.Y.; Dunbar, C.E. The MDS1-EVI1 gene complex as a retrovirus integration site: Impact on behavior of hematopoietic cells and implications for gene therapy. *Mol. Ther.* **2008**, *16*, 439–449. [[CrossRef](#)]
56. Braun, C.J.; Boztug, K.; Paruzynski, A.; Witzel, M.; Schwarzer, A.; Rothe, M.; Modlich, U.; Beier, R.; Göhring, G.; Steinemann, D.; et al. Gene therapy for Wiskott-Aldrich syndrome-long-term efficacy and genotoxicity. *Sci. Transl. Med.* **2014**, *6*, 227ra33. [[CrossRef](#)]
57. Bluebird Bio, Inc. Bluebird bio Reports Second Quarter Financial Results and Provides Operational Update. Press Release. Available online: <https://investor.bluebirdbio.com/news-releases/news-release-details/bluebird-bio-reports-second-quarter-financial-results-and> (accessed on 25 April 2023)
58. Qi, H.; Liu, S.; Guo, C.; Wang, J.; Greenaway, F.T.; Sun, M.Z. Role of annexin A6 in cancer (Review). *Oncol. Lett.* **2015**, *10*, 1947–1952. [[CrossRef](#)] [[PubMed](#)]
59. Bi, X.; Jones, T.; Abbasi, F.; Lee, H.; Stultz, B.; Hursh, D.A.; Mortin, M.A. Drosophila caliban, a nuclear export mediator, can function as a tumor suppressor in human lung cancer cells. *Oncogene* **2005**, *24*, 8229–8239. [[CrossRef](#)] [[PubMed](#)]
60. Scanlan, M.J.; Chen, Y.T.; Williamson, B.; Gure, A.O.; Stockert, E.; Gordan, J.D.; Türeci, O.; Sahin, U.; Pfrendschuh, M.; Old, L.J. Characterization of human colon cancer antigens recognized by autologous antibodies. *Int. J. Cancer* **1998**, *76*, 652–658. [[CrossRef](#)]

61. Chen, L.; Wu, Q.; Xu, X.; Yang, C.; You, J.; Chen, F.; Zeng, Y. Cancer/testis antigen LDHC promotes proliferation and metastasis by activating the PI3K/Akt/GSK-3 $\beta$ -signaling pathway and the in lung adenocarcinoma. *Exp. Cell Res.* **2021**, *398*, 112414. [[CrossRef](#)] [[PubMed](#)]
62. Kong, L.; Du, W.; Cui, Z.; Wang, L.; Yang, Z.; Zhang, H.; Lin, D. Expression of lactate dehydrogenase C in MDA-MB-231 cells and its role in tumor invasion and migration. *Mol. Med. Rep.* **2016**, *13*, 3533–3538. [[CrossRef](#)]
63. O’Neal, J.; Gao, F.; Hassan, A.; Monahan, R.; Barrios, S.; Lee, I.; Chng, W.J.; Vij, R.; Tomasson, M.H. Neurobeachin (NBEA) is a target of recurrent interstitial deletions at 13q13 in patients with MGUS and multiple myeloma. *Exp. Hematol.* **2009**, *37*, 234–244. [[CrossRef](#)]
64. Hattori, M.; Tsukamoto, N.; Nur-e Kamal, M.S.; Rubinfeld, B.; Iwai, K.; Kubota, H.; Maruta, H.; Minato, N. Molecular cloning of a novel mitogen-inducible nuclear protein with a Ran GTPase-activating domain that affects cell cycle progression. *Mol. Cell. Biol.* **1995**, *15*, 552–560. [[CrossRef](#)]
65. Banerjee, R.; Mani, R.S.; Russo, N.; Scanlon, C.S.; Tsodikov, A.; Jing, X.; Cao, Q.; Palanisamy, N.; Metwally, T.; Inglehart, R.C.; et al. The tumor suppressor gene rap1GAP is silenced by miR-101-mediated EZH2 overexpression in invasive squamous cell carcinoma. *Oncogene* **2011**, *30*, 4339–4349. [[CrossRef](#)]
66. Cui, X.; Song, L.; Bai, Y.; Wang, Y.; Wang, B.; Wang, W. Elevated IQGAP1 and CDC42 levels correlate with tumor malignancy of human glioma. *Oncol. Rep.* **2017**, *37*, 768–776. [[CrossRef](#)]
67. White, C.D.; Brown, M.D.; Sacks, D.B. IQGAPs in cancer: A family of scaffold proteins underlying tumorigenesis. *FEBS Lett.* **2009**, *583*, 1817–1824. [[CrossRef](#)]
68. Ma, B.B.; Zhang, T.J.; Wang, C.Z.; Xu, Z.J.; Zhou, J.D.; Gu, Y.; Ma, J.C.; Deng, Z.Q.; Lin, J.; Qian, J. Methylation-independent CRIP1 expression is a potential biomarker affecting prognosis in cytogenetically normal acute myeloid leukemia. *Am. J. Transl. Res.* **2020**, *12*, 4840–4852.
69. Li, M.; Ma, Y.; Zhong, Y.; Liu, Q.; Chen, C.; Qiang, L.; Wang, X. KALRN mutations promote antitumor immunity and immunotherapy response in cancer. *J. Immunother. Cancer* **2020**, *8*, e000293. [[CrossRef](#)] [[PubMed](#)]
70. Heckl, D.; Schwarzer, A.; Haemmerle, R.; Steinemann, D.; Rudolph, C.; Skawran, B.; Knoess, S.; Krause, J.; Li, Z.; Schlegelberger, B.; et al. Lentiviral vector induced insertional haploinsufficiency of EBF1 causes murine leukemia. *Mol. Ther.* **2012**, *20*, 1187–1195. [[CrossRef](#)] [[PubMed](#)]
71. Hirouchi, T.; Takabatake, T.; Yoshida, K.; Nitta, Y.; Nakamura, M.; Tanaka, S.; Ichinohe, K.; Oghiso, Y.; Tanaka, K. Upregulation of c-myc gene accompanied by PU.1 deficiency in radiation-induced acute myeloid leukemia in mice. *Exp. Hematol.* **2008**, *36*, 871–885. [[CrossRef](#)] [[PubMed](#)]
72. Villa, E.; Paul, R.; Meynet, O.; Volturo, S.; Pinna, G.; Ricci, J.E. The E3 ligase UBR2 regulates cell death under caspase deficiency via Erk/MAPK pathway. *Cell Death Dis.* **2020**, *11*, 1041. [[CrossRef](#)]
73. Mao, J.; Liang, Z.; Zhang, B.; Yang, H.; Li, X.; Fu, H.; Zhang, X.; Yan, Y.; Xu, W.; Qian, H. UBR2 Enriched in p53 Deficient Mouse Bone Marrow Mesenchymal Stem Cell-Exosome Promoted Gastric Cancer Progression via Wnt/ $\beta$ -Catenin Pathway. *Stem Cells* **2017**, *35*, 2267–2279. [[CrossRef](#)] [[PubMed](#)]
74. Wang, X.; Rivière, I. Genetic Engineering and Manufacturing of Hematopoietic Stem Cells. *Mol. Ther.-Methods Clin. Dev.* **2017**, *5*, 96–105. [[CrossRef](#)] [[PubMed](#)]
75. Tajer, P.; Canté-Barrett, K.; Naber, B.A.; Vloemans, S.A.; van Eggermond, M.C.; van der Hoorn, M.L.; Pike-Overzet, K.; Staal, F.J. IL3 Has a Detrimental Effect on Hematopoietic Stem Cell Self-Renewal in Transplantation Settings. *Int. J. Mol. Sci.* **2022**, *23*, 2736. [[CrossRef](#)] [[PubMed](#)]
76. Roßmanith, T.; Schröder, B.; Bug, G.; Müller, P.; Klenner, T.; Knaus, R.; Hoelzer, D.; Ottmann, O.G.; Bug, G. Interleukin 3 Improves the Ex Vivo Expansion of Primitive Human Cord Blood Progenitor Cells and Maintains the Engraftment Potential of SCID Repopulating Cells. *Stem Cells* **2001**, *19*, 313–320. [[CrossRef](#)]
77. Uchida, N.; Hsieh, M.M.; Hayakawa, J.; Madison, C.; Washington, K.N.; Tisdale, J.F. Optimal conditions for lentiviral transduction of engrafting human CD34 + cells. *Gene Ther.* **2011**, *18*, 1078–1086. [[CrossRef](#)]
78. Hatzfeld, J.; Li, M.L.; Brown, E.L.; Sookdeo, H.; Levesque, J.P.; O’toole, T.; Gurney, C.; Clark, S.C.; Hatzfeld, A. Release of Early Human Hematopoietic Progenitors from Quiescence by Antisense Transforming Growth Factor $\beta$ 1 or Rb Oligonucleotides. *J. Exp. Med.* **1991**, *174*, 925–929. [[CrossRef](#)]
79. Thompson, N.L.; Flanders, K.C.; Smith, J.M.; Ellingsworth, L.R.; Roberts, A.B.; Sporn, M.B. Expression of transforming growth factor- $\beta$ 1 in specific cells and tissues of adult and neonatal mice. *J. Cell Biol.* **1989**, *108*, 661–669. [[CrossRef](#)]
80. Yamazaki, S.; Iwama, A.; Takayanagi, S.I.; Eto, K.; Ema, H.; Nakauchi, H. TGF- $\beta$  as a candidate bone marrow niche signal to induce hematopoietic stem cell hibernation. *Blood* **2009**, *113*, 1250–1256. [[CrossRef](#)]
81. Challen, G.A.; Boles, N.C.; Chambers, S.M.; Goodell, M.A. Distinct Hematopoietic Stem Cell Subtypes Are Differentially Regulated by TGF- $\beta$ 1. *Cell Stem Cell* **2010**, *6*, 265–278. [[CrossRef](#)]
82. Fortunel, N.; Batard, P.; Hatzfeld, A.; Monier, M.N.; Panterne, B.; Lebkowski, J.; Hatzfeld, J. High Proliferative Potential-Quiescent cells: A working model to study primitive quiescent hematopoietic cells. *J. Cell Sci.* **1998**, *111*, 1967–1875. [[CrossRef](#)]
83. Soma, T.; Yu, J.M.; Dunbar, C.E. Maintenance of Murine Long-Term Repopulating Stem Cells in Ex Vivo Culture Is Affected by Modulation of Transforming Growth Factor- $\beta$ 3 But Not Macrophage Inflammatory Protein-1 Activities. *Blood* **2015**, *87*, 4561–4567. [[CrossRef](#)]

84. Ceccaldi, R.; Parmar, K.; Mouly, E.; Delord, M.; Kim, J.M.; Regairaz, M.; Pla, M.; Vasquez, N.; Zhang, Q.S.; Pondarre, C.; et al. Bone marrow failure in fanconi anemia is triggered by an exacerbated p53/p21 DNA damage response that impairs hematopoietic stem and progenitor cells. *Cell Stem Cell* **2012**, *11*, 36–49. [[CrossRef](#)]
85. Río, P.; Navarro, S.; Wang, W.; Sánchez-Domínguez, R.; Pujol, R.M.; Segovia, J.C.; Bogliolo, M.; Merino, E.; Wu, N.; Salgado, R.; et al. Successful engraftment of gene-corrected hematopoietic stem cells in non-conditioned patients with Fanconi anemia. *Nat. Med.* **2019**, *25*, 1396–1401. [[CrossRef](#)]
86. Zhang, H.; Kozono, D.E.; O'Connor, K.W.; Vidal-Cardenas, S.; Rousseau, A.; Hamilton, A.; Moreau, L.; Gaudio, E.F.; Greenberger, J.; Bagby, G.; et al. TGF- $\beta$  inhibition rescues hematopoietic stem cell defects and bone marrow failure in Fanconi anemia. *Cell Stem Cell* **2016**, *18*, 668–681. [[CrossRef](#)] [[PubMed](#)]
87. Rodríguez, A.; Yang, C.; Furutani, E.; García de Teresa, B.; Velázquez, M.; Filiatrault, J.; Sambel, L.A.; Phan, T.; Flores-Guzmán, P.; Sánchez, S.; et al. Inhibition of TGF $\beta$ 1 and TGF $\beta$ 3 promotes hematopoiesis in Fanconi anemia. *Exp. Hematol.* **2021**, *93*, 70–84. [[CrossRef](#)] [[PubMed](#)]
88. U.S. Food and Drug Administration. *Guidance for Industry Preclinical Assessment of Investigational Cellular and Gene Therapy Products Additional*; Food and Drug Administration: Rockville, MD, USA, 2013. Available online: <https://www.fda.gov/media/87564/download> (accessed on 22 March 2023)
89. Cornetta, K.; Lin, T.Y.; Pellin, D.; Kohn, D.B. Meeting FDA Guidance recommendations for replication-competent virus and insertional oncogenesis testing. *Mol. Ther.-Methods Clin. Dev.* **2023**, *28*, 28–39. [[CrossRef](#)] [[PubMed](#)]
90. Yuasa, H.; Oike, Y.; Iwama, A.; Nishikata, I.; Sugiyama, D.; Perkins, A.; Mucenski, M.L.; Suda, T.; Morishita, K. Oncogenic transcription factor Evi1 regulates hematopoietic stem cell proliferation through GATA-2 expression. *EMBO J.* **2005**, *24*, 1976–1987. [[CrossRef](#)] [[PubMed](#)]
91. Zhang, Y.; Stehling-Sun, S.; Lezon-Geyda, K.; Juneja, S.C.; Coillard, L.; Chatterjee, G.; Wuertzer, C.A.; Camargo, F.; Perkins, A.S. PR-domain—Containing Mds1-Evi1 is critical for long-term hematopoietic stem cell function. *Blood* **2011**, *118*, 3853–3861. [[CrossRef](#)]
92. Kataoka, K.; Sato, T.; Yoshimi, A.; Goyama, S.; Tsuruta, T.; Kobayashi, H.; Shimabe, M.; Arai, S.; Nakagawa, M.; Imai, Y.; et al. Evi1 is essential for hematopoietic stem cell self-renewal, and its expression marks hematopoietic cells with long-term multilineage repopulating activity. *J. Exp. Med.* **2011**, *208*, 2403–2416. [[CrossRef](#)] [[PubMed](#)]
93. Voit, R.A.; Tao, L.; Yu, F.; Cato, L.D.; Cohen, B.; Fleming, T.J.; Antoszewski, M.; Liao, X.; Fiorini, C.; Nandakumar, S.K.; et al. nature immunology A genetic disorder reveals a hematopoietic stem cell regulatory network co-opted in leukemia. *Nat. Immunol.* **2023**, *24*, 69–83. [[CrossRef](#)]
94. Birdwell, C.; Fiskus, W.; Kadia, T.M.; DiNardo, C.D.; Mill, C.P.; Bhalla, K.N. EVI1 dysregulation: Impact on biology and therapy of myeloid malignancies. *Blood Cancer J.* **2021**, *11*, 64. [[CrossRef](#)] [[PubMed](#)]
95. Caron, M.C.; Caruso, M. A nuclear localization signal in the matrix of spleen necrosis virus (SNV) does not allow efficient gene transfer into quiescent cells with SNV-derived vectors. *Virology* **2005**, *338*, 292–296. [[CrossRef](#)] [[PubMed](#)]
96. Roe, T.; Reynolds, T.C.; Yu, G.; Brown, P.O. Integration of murine leukemia virus DNA depends on mitosis. *EMBO J.* **1993**, *12*, 2099–2108. [[CrossRef](#)] [[PubMed](#)]
97. Li, Z.; Schwiager, M.; Lange, C.; Kraunus, J.; Sun, H.; van den Akker, E.; Modlich, U.; Serinsöz, E.; Will, E.; von Laer, D.; et al. Predictable and efficient retroviral gene transfer into murine bone marrow repopulating cells using a defined vector dose. *Exp. Hematol.* **2003**, *31*, 1206–1214. [[CrossRef](#)] [[PubMed](#)]
98. Zhang, C.C.; Lodish, H.F. Murine hematopoietic stem cells change their surface phenotype during ex vivo expansion. *Blood* **2005**, *105*, 4314–4320. [[CrossRef](#)]

**Disclaimer/Publisher's Note:** The statements, opinions and data contained in all publications are solely those of the individual author(s) and contributor(s) and not of MDPI and/or the editor(s). MDPI and/or the editor(s) disclaim responsibility for any injury to people or property resulting from any ideas, methods, instructions or products referred to in the content.